

PROBING THE COEVOLUTION OF SUPERMASSIVE BLACK HOLES AND GALAXIES USING GRAVITATIONALLY LENSED QUASAR HOSTS¹

CHIEN Y. PENG^{2,3,4}, CHRIS D. IMPEY⁴, HANS-WALTER RIX⁵, CHRISTOPHER S. KOCHANNEK⁶, CHARLES R. KEETON^{7,8}, EMILIO E. FALCO⁷, JOSEPH LEHÁR^{7,9}, & BRIAN A. MCLEOD⁷

Draft version July 18, 2018

ABSTRACT

In the present-day universe, supermassive black hole masses (\mathcal{M}_{BH}) appear to be strongly correlated with their galaxy's bulge luminosity, among other properties. In this study, we explore the analogous relationship between \mathcal{M}_{BH} , derived using the virial method, and the stellar R -band bulge luminosity (L_R) or stellar bulge mass (\mathcal{M}_*) at epochs of $1 \lesssim z \lesssim 4.5$ using a sample of 31 gravitationally lensed AGNs and 20 non-lensed AGNs. At redshifts $z > 1.7$ (10–12 Gyrs ago), we find that the observed $\mathcal{M}_{\text{BH}}-L_R$ relation is nearly the same (to within ~ 0.3 mag) as it is today. When the observed L_R are corrected for luminosity evolution, this means that the black holes grew in mass faster than their hosts, with the $\mathcal{M}_{\text{BH}}/\mathcal{M}_*$ mass ratio being a factor of $\gtrsim 4_{-1}^{+2}$ times larger at $z > 1.7$ than it is today. By the redshift range $1 \lesssim z \lesssim 1.7$ (8–10 Gyrs ago), the $\mathcal{M}_{\text{BH}}/\mathcal{M}_*$ ratio is at most two times higher than today, but it may be consistent with no evolution. Combining the results, we conclude that the ratio $\mathcal{M}_{\text{BH}}/\mathcal{M}_*$ rises with look-back time, although it may saturate at ≈ 6 times the local value. Scenarios in which moderately luminous quasar hosts at $z \gtrsim 1.7$ were fully formed bulges that passively faded to the present epoch are ruled out.

Subject headings: galaxies: evolution — galaxies: quasars — galaxies: fundamental parameters — galaxies: structure — galaxies: bulges

1. INTRODUCTION

A remarkable discovery over the last decade is the existence of strong correlations between the masses \mathcal{M}_{BH} of supermassive black holes (BHs) and the overall properties of the host galaxy bulge, in particular the luminosity, stellar mass (\mathcal{M}_*) and stellar velocity dispersion (σ_*) (e.g., Kormendy & Richstone 1995; Magorrian et al. 1998; Ho 1999; Gebhardt et al. 2000a; Ferrarese & Merritt 2000; Kormendy & Gebhardt 2001, Marconi & Hunt 2003, Häring & Rix 2004). There are also correlations with the narrow [O III] line width (Shields et al. 2003, Boroson 2003), and with the central stellar density profiles of the bulges (Graham et al. 2001). The small intrinsic scatter, especially in the correlation between \mathcal{M}_{BH} and the host's stellar velocity dispersion, mass, and luminosity, suggests that supermassive black hole growth and galaxy evolution are coupled processes. An empirical approach to understanding this coupling is to trace these correlations to earlier epochs, determining

whether the tight correlations developed recently or long ago, and measuring the relative growth rates of black holes and stellar bulges. Unfortunately, it is impossible to estimate BH masses beyond the local universe with the most robust tool – spatially resolved kinematics. Also, it is very difficult to measure stellar velocity dispersions at redshifts $z \gtrsim 1$ in normal galaxies.

The most straightforward correlation to extend to high redshifts ($z \geq 1$) is the BH mass-bulge luminosity relation. The correlation between \mathcal{M}_{BH} and galaxy luminosity, originally noted by Kormendy & Richstone (1995) for nearby, normal galaxies, has now been explored in great detail and measured in passbands from the optical to the near infrared (e.g. Magorrian et al. 1998; Ho 1999; Kormendy & Gebhardt 2001; Laor 2001; Merritt & Ferrarese 2001; Erwin, Graham, & Caon 2002, McLure & Dunlop 2002; Bettoni et al. 2003; Marconi & Hunt 2003, Ivanov & Alonso-Herrero 2003). These relationships are fairly tight, with a typical scatter of 0.3-0.45 dex in BH mass for early-type galaxies or early-type spiral galaxies that can be reliably decomposed into a bulge and a disk (Erwin, Graham, & Caon 2002, Bettoni et al. 2003; Marconi & Hunt 2003). After two decades of ground-based and *HST* studies of quasar hosts at low ($z \approx 0$) and intermediate ($z \leq 1$) redshifts studies have found that AGN hosts and normal galaxies share many of the same characteristics (e.g. Hutchings Crampton, & Campbell 1984; Gehren et al. 1984; Neugebauer et al. 1985; Lehnert et al. 1992; McLeod & Rieke 1994, McLeod 1995; Lawrence 1999; Nelson 2000; Wang, Biermann, & Wandel 2000): they look alike in gross appearance. The ubiquity of supermassive black holes in galaxies suggests that most or all normal galaxies experience an AGN phase at some point in their development. And this AGN activity might itself have a role in regulating star formation, which would affect the development of early-type galaxies (Di Matteo,

¹ Based on observations with the NASA/ESA *Hubble Space Telescope*, obtained at the Space Telescope Science Institute, which is operated by AURA, Inc., under NASA contract NAS5-26555.

³ STScI Fellow

⁴ Current address: Space Telescope Science Institute, 3700 San Martin Drive, Baltimore, MD 21218; cyp@stsci.edu.

⁵ Steward Observatory, University of Arizona, 933 N. Cherry Av., Tucson, AZ 85721; cimpey@as.arizona.edu.

⁶ Max-Planck-Institut für Astronomie, Königstuhl 17, Heidelberg, D-69117, Germany; rix@mpia.de

⁷ The Ohio State University, 4055 McPherson Lab, 140 West 18th Avenue, Columbus, OH 43210

⁸ Harvard-Smithsonian Center for Astrophysics, 60 Garden Street, Cambridge, MA 02138; falco, jlehar, bmcLeod@cfa.harvard.edu

⁹ Current address: Department of Physics & Astronomy, Rutgers University, 136 Frelinghuysen Road, Piscataway, NJ 08854

⁹ Current address: CombinatorRx, Inc., 650 Albany Street, Boston, MA 02118; lehar@rcn.com

Springel, Herquist 2005; Ho 2005; Somerville et al. in prep.).

Studying the BH–bulge luminosity relation at high redshift requires measuring both quantities in bright AGNs with comparatively faint hosts. The AGN activity allows \mathcal{M}_{BH} to be estimated using the so-called virial technique (see Ho 1999; Wandel, Peterson, & Malkan 1999, Kaspi et al. 2000, McLure & Jarvis 2002, Vestergaard 2002, Peterson et al. 2004, Kaspi et al. 2005). Reverberation mapping (Blandford & McKee 1982; Peterson 1993) of nearby AGN provides a correlation between broad-line region (BLR) sizes and AGN continuum luminosity (Kaspi et al. 2000, Kaspi et al. 2005). Combined with line widths, this virial mass can be normalized to the local $\mathcal{M}_{\text{BH}}\text{-}\sigma_*$ relation to provide estimates of \mathcal{M}_{BH} . These have been explored in detail locally (Gebhardt et al. 2000b; Ferrarese et al. 2001; Nelson et al. 2004, Onken et al. 2004; Barth, Greene, & Ho 2005a; Greene & Ho 2005, Kaspi et al. 2005) and should work also at higher redshift. What is harder to measure is the luminosity of the host galaxy bulge; AGN activity and cosmological surface brightness dimming make it difficult to detect distant AGN hosts, let alone measure their properties. To date, 70 orbits on *HST* have been used to image just 15 objects at $z \approx 2$ in the NICMOS *H*-band (Kukula et al. 2001, Ridgway et al. 2001). Despite this modest sample size, it is already possible to study the BH–bulge relationship, and Peng et al. (2005, P06 hereafter) show that these high redshift systems nearly lie on the local \mathcal{M}_{BH} versus rest-frame bulge luminosity relationship in the *R*-band. If the bulges at $z \simeq 2$ are fully formed and passively fading, this implies that the mean $\mathcal{M}_{\text{BH}}/\mathcal{M}_*$ ratio is a factor of 3–6 higher at $z \gtrsim 2$ than today. The amount of evolution is even larger if the hosts are analogous to coeval inactive galaxies, which have lower mass-to-light (\mathcal{M}/L) ratios than at the present epoch due to their younger stellar populations (e.g. Rudnick et al. 2003). This implies that initially black holes must have grown faster than their bulges, with the bulges playing “catch-up” from $z \gtrsim 2$ to the present. Indeed this evolution may still be observable in $z \approx 0.4$ Seyfert galaxies (Treu, Malkan, & Blandford 2004), although the effect is smaller. The conclusions inferred from the high redshift study of P06, however, were tentative because of the small sample size, covering two thin redshift slices with only 15 objects.

Several other lines of evidence suggest that the host galaxies developed more slowly at early epochs than their central black holes. McLure et al. (2005) find similar evolution to the results of P06 by comparing *radio galaxy* luminosities to *quasar* black hole masses. There are risks, however, in drawing inferences by comparing the properties of hosts and black holes in potentially different types of objects. Using CO lines to estimate the stellar velocity dispersion σ_* in high redshift quasar hosts, Shields, Salvander, & Bonning (2005) also find tentative evidence that the hosts are undermassive compared to their central BHs. The same conclusion is reached by Merloni, Rudnick, & Di Matteo (2004) who compared the star formation rate density and stellar mass density in the universe with accretion rates of AGNs. However, several other studies tell a conflicting story. Using the [O III] line width to approximate σ_* , Shields et al. (2003) find little change in the $\mathcal{M}_{\text{BH}}\text{-}\sigma_*$ relation with redshift, albeit with a large scatter. Finally, in contrast to all these

studies, Borys et al. (2005) find that the $\mathcal{M}_{\text{BH}}/\mathcal{M}_*$ ratio may be 1–2 order of magnitude *smaller* in high redshift submillimeter selected galaxies than today, suggesting that BH masses must grow rapidly from $z \approx 2$. However, their finding is based on assuming that their low luminosity AGNs are *all* radiating at the Eddington limit, which places a lower limit on the BH mass. In practice, the Eddington ratios in AGNs are observed to span anywhere from near 0 for normal galaxies to unity (Woo & Urry 2002), and there are abundant examples of gas rich galaxies that have no detectable AGN. Because of the complications of these other techniques, the most promising way to quantify the evolution of $\mathcal{M}_{\text{BH}}/\mathcal{M}_*$ is still to measure \mathcal{M}_{BH} and the host luminosity in the same objects. To do so, however, requires a much larger sample than is currently available in the literature.

Here we improve on the number statistics by using gravitationally lensed host galaxies to expand our analysis to 51 objects (see Fig. 1). Gravitational lensing stretches the host galaxy out from underneath the quasar emission, preserving the surface brightness of the host but stretching and distorting its shape, leading to an enormous gain in surface brightness contrast between the host and the quasar compared to unlensed systems. The distortion of the host into an Einstein ring also gives the image of the host a dramatically different morphology from that of any errors in the point spread function (PSF), so the photometry of the host is significantly less susceptible to systematic problems in the PSF model. Thus, while Kukula et al. (2001) and Ridgway et al. (2001) found it challenging to quantify the structure of $z \simeq 2$ hosts even with five-orbit *HST* images, many single orbit images of lensed hosts are easily analyzed because the hosts are observed as luminous arcs and Einstein rings on scales of 1–10 arcsec (see Figures 2–6; also Keeton et al. 2000, Kochanek et al. 1999, Lehár et al. 2000). Given the existence of ~ 80 lensed quasars, *HST* images of lensed quasars are by far the most efficient way of expanding studies of quasar host galaxies, especially at $z \approx 2 - 4$.

In the present study, we measure the rest-frame *R*-band (L_R) luminosities of 31 lensed + 5 unlensed host galaxies from the CASTLES (CfA-Arizona Space Telescope Lens Survey) project, and combine the results with the sample of 15 quasars from Kukula et al. (2001) and Ridgway et al. (2001) that we discussed in P06. We estimate \mathcal{M}_{BH} for the sources using the virial method, and then explore the evolution of the ratio between \mathcal{M}_{BH} and both the rest frame *R*-band bulge luminosity L_R and the estimated stellar mass \mathcal{M}_* between $z \simeq 1$ and $z \simeq 4.5$ given conservative models for the stellar populations and their evolution. In Section 2 we describe the lens data and analysis, summarize the P06 sample, and present our approach to making *k*-corrections. In Section 3 we estimate the BH masses using the virial technique. Section 4 presents the results. Finally, we conclude in Section 5 with a discussion of the evolution of the $\mathcal{M}_{\text{BH}}/\mathcal{M}_*$ ratio from $z \simeq 4.5$ to today. An Appendix discusses systematic uncertainties and explains why they do not affect our conclusions. In particular, we discuss assumptions made about the host galaxy stellar population and evolution (Appendix A), the accuracy of the lens models (B), their complexity (C), and lastly, specifics on several problematic objects (D). All the results assume a standard cos-

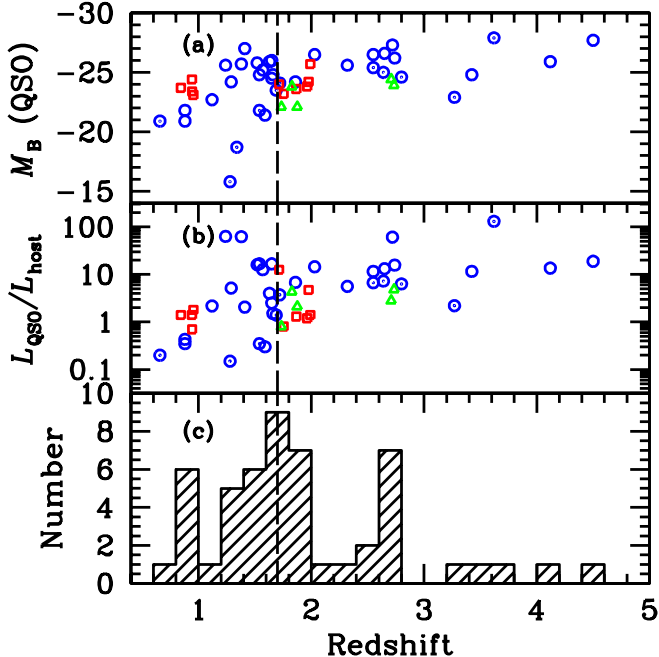


FIG. 1.— Summary of the quasars used in this sample. We include gravitational lenses from the CASTLES project (circles are 2-image lenses; circle-dot are 4-image lenses), and from direct NIC2 imaging studies by Kukula et al. (2001, red squares) and Ridgway et al. (2001, triangles). The dashed line at $z = 1.7$ separates our high and low redshift samples into two bins, each covering approximately 2 Gyrs of look-back time. Panel *a* shows the *B*-band absolute magnitude of the quasar, *b* shows the *H*-band ratio between the quasar and host luminosities, and *c* shows the redshift histogram.

mology with $H_0 = 70 \text{ km}^{-1} \text{ s}^{-1} \text{ Mpc}^{-1}$, $\Omega_m = 0.3$, and $\Omega_\Lambda = 0.7$. The photometry is in the Vega system and is corrected for Galactic extinction using the models of Schlegel, Finkbeiner & Davis (1998).

2. GRAVITATIONAL LENS DATA AND MODELING

In this paper we analyze the host galaxies of lensed quasars observed with *HST* as part of the CfA/Arizona Space Telescope Lens Survey (CASTLES), focusing on those that have both NICMOS/NIC2 *H*-band (F160W) images¹⁰, and published spectra for estimating BH masses. The *V*-band (F555W) and *I*-band (F814W) images obtained as part of CASTLES reflect the rest-frame near- to far-UV radiation and will only be used in a later study. We restricted the analysis to lenses with Einstein ring diameters exceeding $0''.8$ in order to simplify modeling the images to determine the properties of the host galaxy. This choice corresponds to setting a minimum mass for the lens galaxy, and should introduce no biases in the properties of the host galaxy of the quasar source. The data were reduced as detailed by Lehár et al. (2000). For most targets we have only single orbit observations, but a few sources have longer, five orbit observations.

Table 1 summarizes the CASTLES dataset. While this sample includes 31 lensed objects there are 5 which are unlensed: the host galaxy of quasar C in the field of the lensed quasar LBQS 1009–0252 (Hewett et al. 1994); two binary quasar pairs MGC 2214+3550 (Muñoz et al.

1998) and RXJ 0921+4258 (Muñoz et al. 2001). We have reclassified this last system as a binary quasar based on the properties of the host galaxy (see Appendix D). We complemented this sample by including the unlensed 15 objects from Kukula et al. (2001) and Ridgway et al. (2001), summarized in Table 2. Their estimated *H*-band fluxes are published previously (Kukula et al. 2001, Ridgway 2001) and corrected by P06 for morphological corrections and extinction. The full sample consists of 51 hosts spread over the redshift range 1–4.5. We will present a survey of the host galaxy morphologies and colors in a separate study.

We deliberately excluded observations of unlensed host galaxies for which the only available data were at optical rather than near-IR wavelengths (e.g., Aretxaga, Terlevich, & Boyle 1998; Lehnert et al. 1999; Hutchings et al. 2002; Hutchings 2003, Sánchez et al. 2004, Jahnke et al. 2004). These (rest-frame) ultraviolet observations are very sensitive to star formation rates and extinction internal to the host galaxy, which makes *k*-corrections very uncertain, and they are not easily compared to local correlations. We also excluded ground-based near-infrared results (e.g. Falomo, Kotilainen & Treves 2001, Lacy et al. 2002, Sánchez & González-Serrano 2003, and Kuhlbrodt et al. 2005) in favor of a uniform analysis based on *HST* observations.

2.1. Image Modeling

We determine the host galaxy properties given in Tables 1 and 2 by fitting a model to the image using either GALFIT (for unlensed sources, Peng et al. 2002) or LENSFIT (for lensed sources). LENSFIT is a version of GALFIT that has been extended to fit lensed host galaxies while optimizing the mass model for the lens galaxy. Briefly, a LENSFIT model comprises Sérsic (1968) models for the lens galaxy and quasar host galaxy, and point images of the quasar. The quasar and host are distorted by a lens mass model consisting of one or more singular isothermal ellipsoids (SIE) in an external shear field. The model is convolved with the point spread function (PSF) and fitted to the observations. All the model parameters, both for the luminous components and the lens mass model, are simultaneously optimized using the Levenberg-Marquardt non-linear least squares method as implemented by Press et al. (1992). The parameter uncertainties include all covariances among model parameters. As discussed in the Appendix, lensing introduces no significant systematic uncertainties in the measurements of the quasar host galaxies.

We model the light profiles of both the foreground lensing galaxies and the background host galaxies (the “source”) using the Sérsic (1968) model,

$$\Sigma(r) = \Sigma_e \exp \left(-\kappa(n) \left[\left(\frac{r}{r_e} \right)^{1/n} - 1 \right] \right). \quad (1)$$

The Sérsic profile is widely used because it reliably models galaxy light profiles and smoothly covers the range of profile shapes from exponential disks ($n = 1$) to de Vaucouleurs profiles ($n = 4$). The scale length r_e is defined to be the half-light radius of the profile, so the coefficient $\kappa(n)$ is the function of concentration n needed to maintain this definition (see Peng et al. 2002 for details). We use elliptical Sérsic profiles, so there are a total of 7 parameters: the position, the flux scale Σ_e , the half-light

¹⁰ The *H*-band zeropoints are $H_{zpt} = 21.79$ for data obtained prior to year 2000, and $H_{zpt} = 22.11$ post 2000.

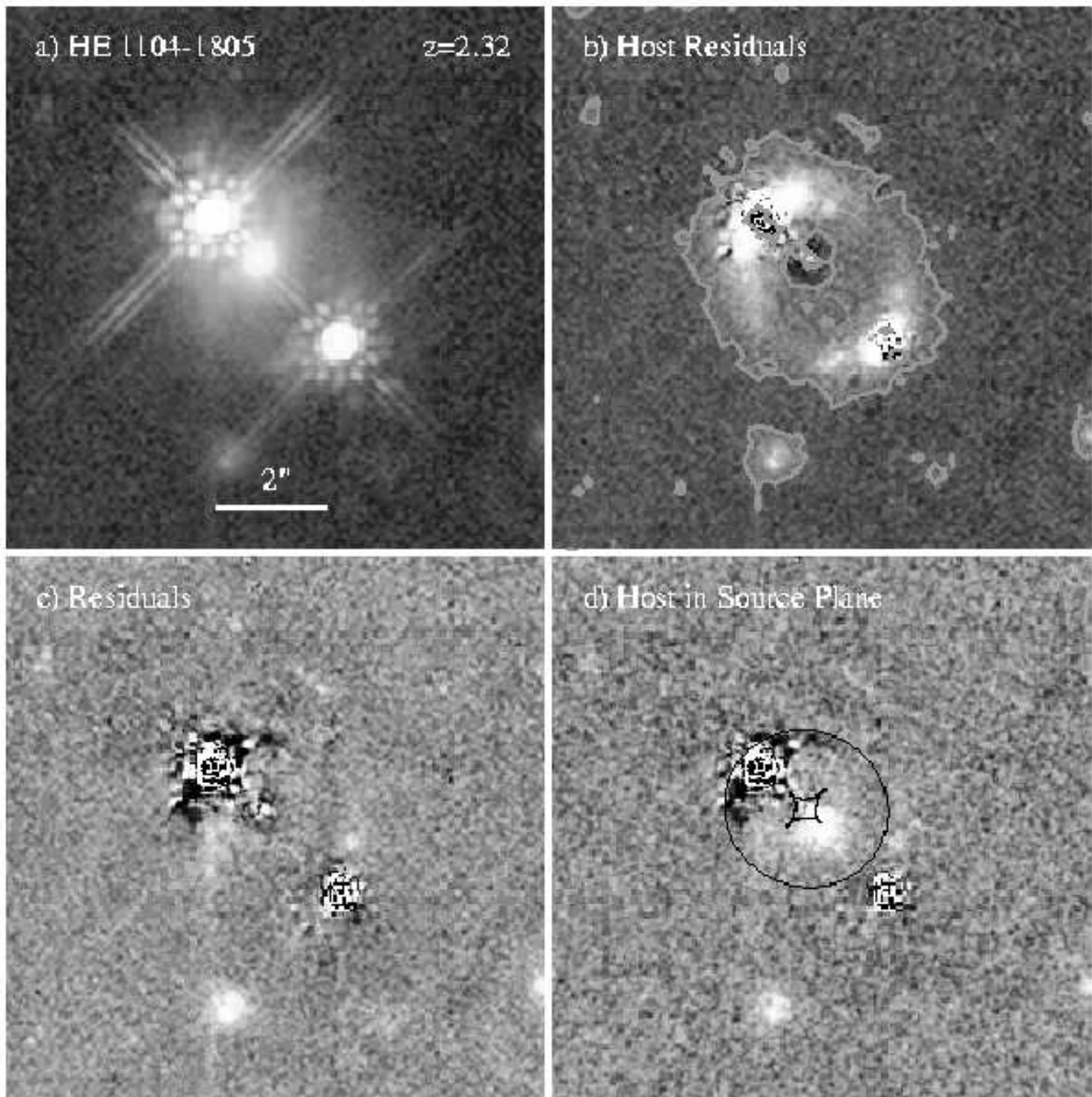


FIG. 2.— The two image lens HE 1104–1805 of a $z = 2.32$ quasar produced by a $z = 0.73$ lens galaxy. Panel *a* shows the original data, Panel *b* shows the lensed host galaxy found after subtracting the lens and quasar components of the best fitting photometric model, Panel *c* shows the residuals from that photometric model, and Panel *d* shows what the unlensed host galaxy would look like in a similar exposure after perfectly subtracting the flux from the quasar. In this 5 orbit exposure, the host, which we estimate to be a galaxy with concentration $n = 2$ and effective radius $r_e = 2.5$ kpc, is observed as a complete Einstein ring. The curves shown superposed on the model of the host galaxy are the lensing caustics.

radius r_e , the concentration n , the axis ratio q and the position angle θ of the major axis. In the absence of lensing, this procedure is identical to the approach used in many studies of host galaxies (e.g. McLure et al. 1999, McLeod & McLeod 2001, Peng et al. 2002, Dunlop et al. 2003, Sánchez et al. 2005, Jahnke et al. 2005).

Like all other studies of quasar hosts, fitting the data requires a good model for the PSF. However, the details are much less important to lensed hosts than unlensed

hosts, because lensed hosts are much more extended and have structures that differ dramatically from the PSF. For example, small errors in the width of the PSF are an enormous problem for analyzing unlensed hosts but have almost no effect on the estimated properties of a host seen as an Einstein ring. This is an important advantage of using lensed hosts – even though *HST* produces very stable PSFs, matching them to quasars is difficult because quasars and stars have different spectral shapes in the in-

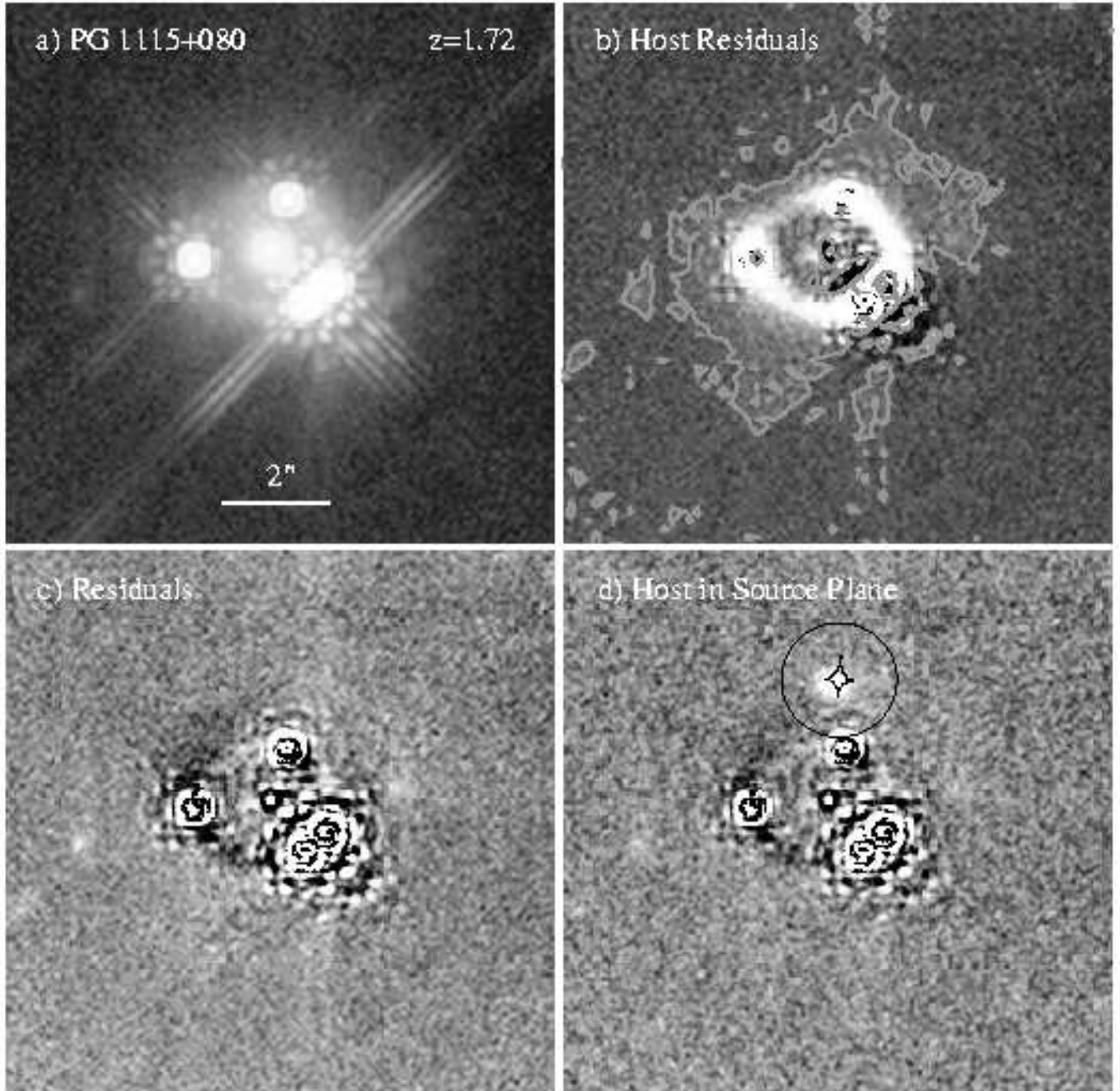


FIG. 3.— The four image lens PG 1115+080 of a $z = 1.72$ quasar produced by a $z = 0.31$ lens galaxy. The panels are described in Fig. 2. In this case we estimate that the host has a concentration of $n = 4$ and an effective radius of $r_e \simeq 1.5$ kpc. The large apparent spatial displacement between the caustics from the center of the lensing galaxy is due to the gravitational influence of a neighboring galaxy external to the field of view, whose lensing effect is represented by a singular isothermal sphere mass model (Impey et al. 1998).

frared. We test for PSF-related problems and biases for the parameters of hosts near our detection thresholds by doing the fits using a collection of 13 high signal-to-noise images of stars. We fit each system with all PSF models, presenting the results for the PSF producing the best fit to the data.

The one challenge of this study, and the main difference from unlensed studies, is that the apparent geometry of the host galaxy and quasar images must be reproduced by a gravitational lens model. As a problem in image fitting, this is merely an inconvenience, since all the lens does is to remap the “unlensed” source plane

coordinates \vec{u} onto the “lensed” lens plane coordinate \vec{x} . On the source plane the host galaxy can again be modeled by an analytic profile $\Sigma(\vec{u})$. Since gravitational lensing conserves surface brightness, the surface brightness of the lensed host is simply $\Sigma(\vec{x}) = \Sigma(\vec{u})$. Given a model for the lens potential $\phi(\vec{x})$ in appropriate units, the lens equation,

$$\vec{u} = \vec{x} - \vec{\nabla}_{\vec{x}}\phi(\vec{x}). \quad (2)$$

gives the mapping from source to lens plane coordinates (Schneider, Ehlers, & Falco 1992). The remapping re-

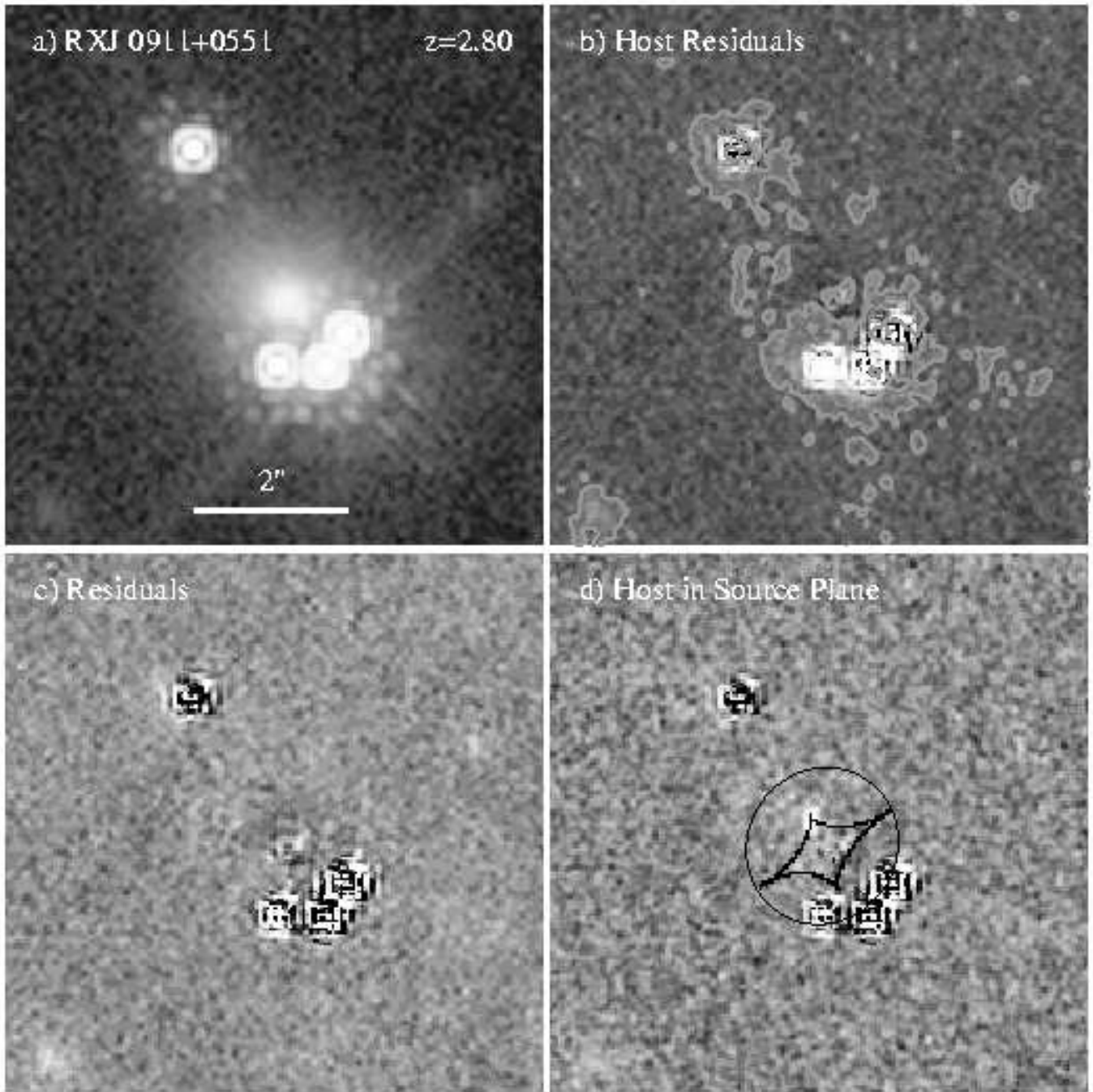


FIG. 4.— The four image lens RXJ 0911+0551 of a $z = 2.8$ quasar produced by a $z = 0.77$ lens galaxy. The panels are described in Fig. 2. In this case we estimate that the host has an effective radius of $r_e \simeq 1 - 2$ kpc..

quires a lens model. We outline our modeling procedure here, leaving more detailed discussion to a later study (Peng et al. in preparation). We model the lens as one or more singular isothermal ellipsoids (SIE) in an external (tidal) shear field. The SIE has a projected mass density of

$$\kappa(x, y) = \frac{b}{2} \left[\frac{2q^2}{1+q^2} (x^2 + y^2/q^2) \right]^{-1/2}, \quad (3)$$

specified by a mass scale b , an axis ratio q and a major axis position angle. The parameter b is approximately

the radius of the Einstein ring the lens will form, although the relation is exact only for $q = 1$ (see Kochanek, Keeton, & McLeod 2001). The tidal shear, as its name suggests, is needed to model the tidal effects from objects near the lens or along the line of sight to the quasar (Keeton, Kochanek, & Seljak 1997). The parameters of the lens model are adjusted as part of fitting the data.

For the types of systems we consider, the geometry of the lensed images and the host galaxy constrain the parameters of the lens model quite accurately. Moreover their uncertainties have little effect on the conclusions, and the lensed images are well-fit by the model. Indeed,

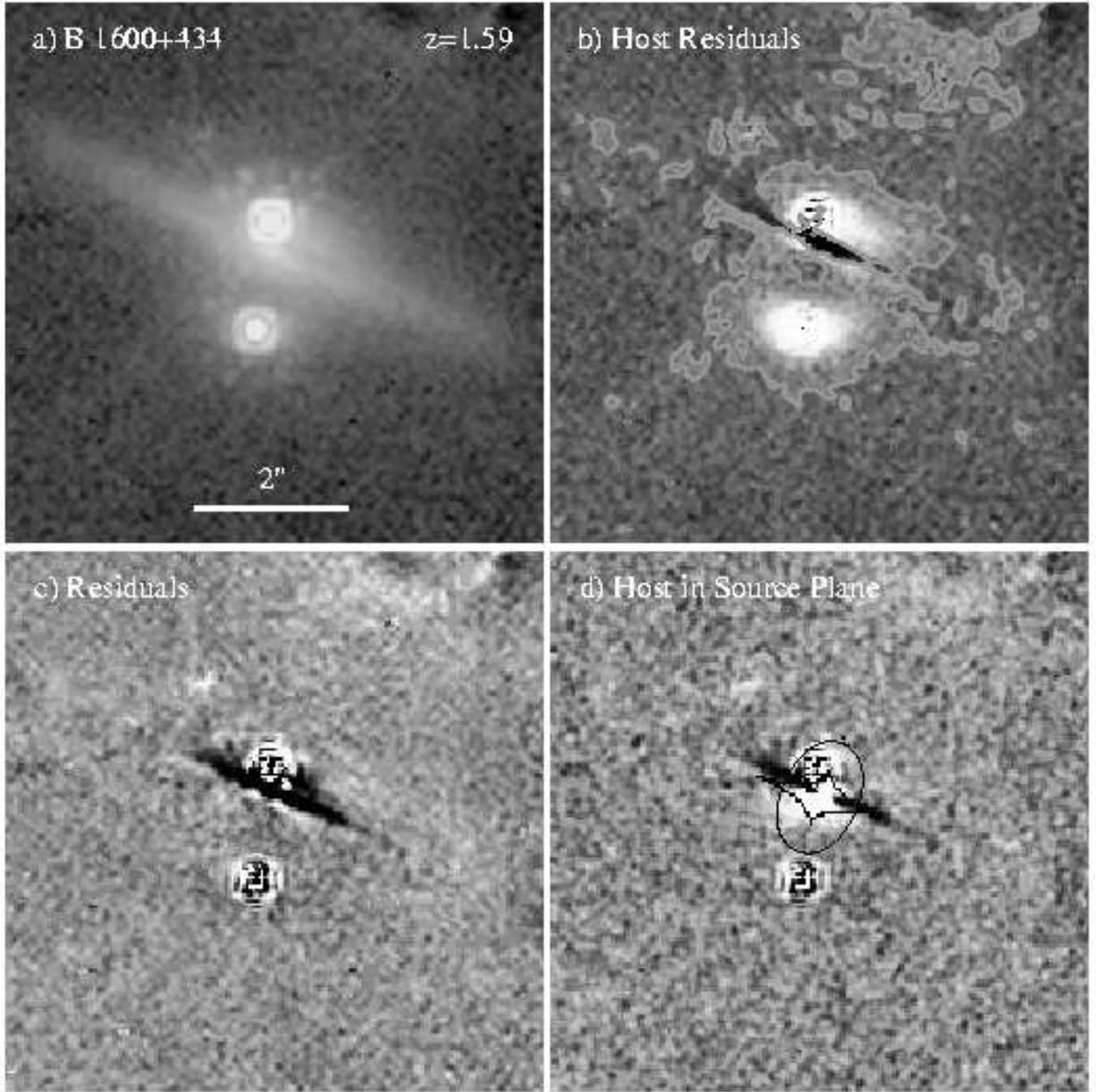


FIG. 5.— The two image lens B 1600+434 of a $z = 1.59$ quasar produced by a $z = 0.41$, edge-on spiral lens galaxy. The panels are described in Fig. 2. In this case we estimate that the host has an effective radius of $r_e \simeq 3$ kpc.

the random and systematic uncertainties of the host photometry due to PSF issues are significantly larger than uncertainties due to the lens model. This, combined with the diminished importance of the character of the PSF, is what give lensing its much greater sensitivity to hosts relative to direct imaging. To reassure readers unfamiliar with lens models, we discuss this further in Appendices B and C.

Figure 1 summarizes the luminosity, quasar/host contrast and redshift distribution of the full sample. In general, the unlensed quasars of Kukula et al. (2001) and Ridgway et al. (2001) were selected to be lower luminos-

ity AGNs, while the lenses are a heterogeneous sample drawn from a broad range of optical- and radio-selected lens surveys with differing sensitivities. The benefit of the lensing magnification is easily apparent in Figure 1 — we can probe to higher average quasar luminosities and quasar/host galaxy contrast levels than with the unlensed quasars. We can also measure the concentration index n of roughly 80% of the lensed hosts (the other 20% are held fixed to $n = 4$), despite the relatively shallow data (1-orbit) available for most of the objects (Peng et al. 2006, in preparation). We have size estimates for all lensed hosts with luminosity measurements, whereas

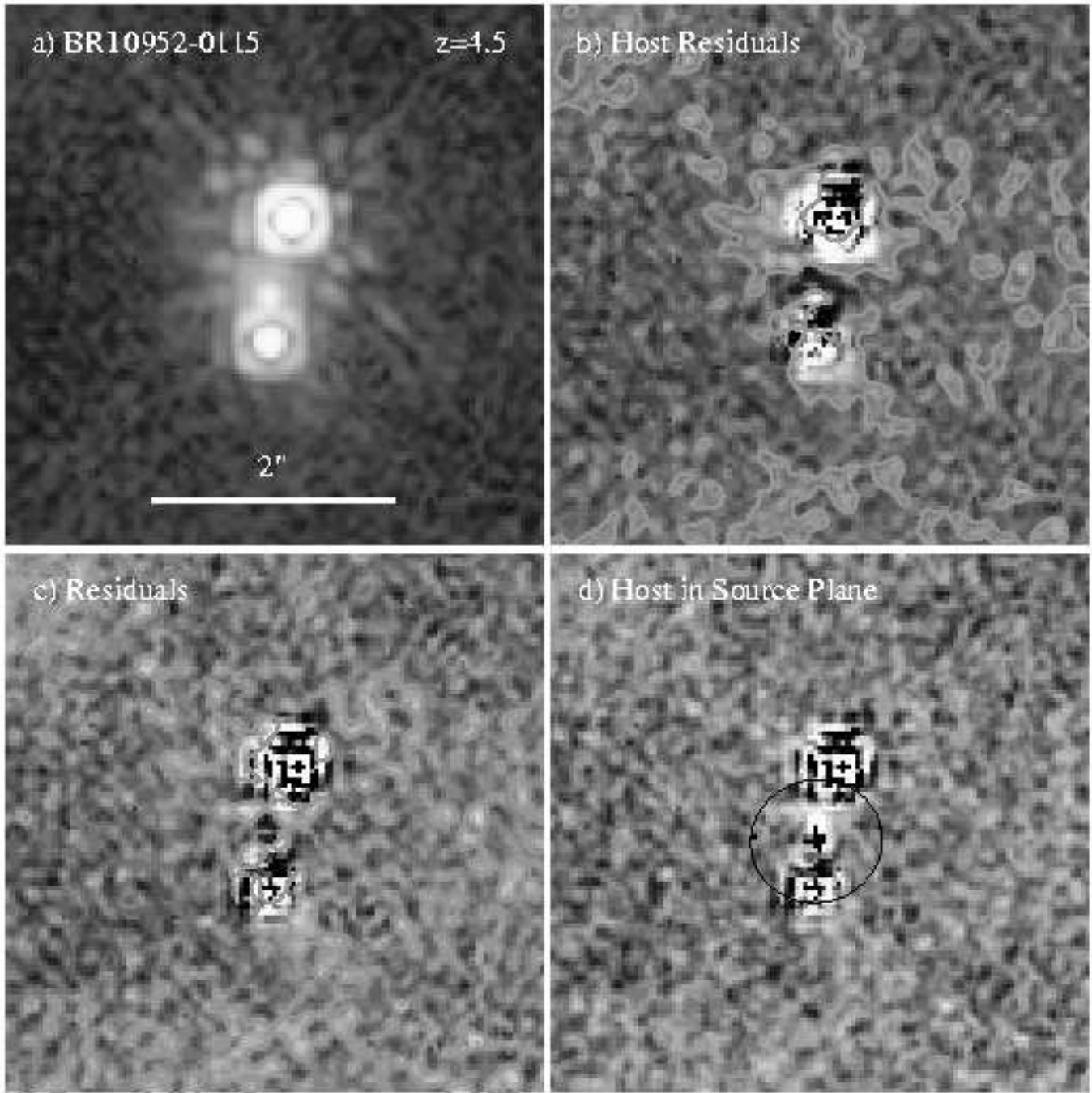


FIG. 6.— The two image lens BRI 0952–0115 of a $z = 4.5$ quasar produced by a $z \approx 0.41$ lens galaxy. The panels are described in Fig. 2. The host is resolved into an arc. In this case we estimate that the host has an effective radius of $r_e \lesssim 1$ kpc.

they are poorly constrained in the absence of lensing, despite their longer integration times (Kukula et al. 2001, Ridgway et al. 2001).

Figures 2–6 illustrate five examples of lensed hosts: HE 1104–1805 ($z_s = 2.32$), PG 1115+080 ($z_s = 1.72$), RXJ 0911+0551 ($z_s = 2.80$), B 1600+434 ($z_s = 1.59$), BRI 0952–0115 ($z_s = 4.5$). With the exception of the one-orbit observation of BRI 0952–0115, these are all examples of the deeper five-orbit observations. For each lens we show the raw data, the structure of the lensed host after using the best fit model to subtract the contributions from the lens galaxy and the quasar

point sources, and the final residuals from subtracting the full model. We also show a model, including noise, of what the host would look like in a comparable HST image if it had not been gravitationally lensed and assuming perfect subtraction of the quasar point source flux. The lensed hosts not only gain from a net magnification of their flux (by factors of 8, 18, 7, 4 and 8 for HE 1104–1805, PG 1115+080, RXJ 0911+0551, B 1600+434, and BRI 0952–0115, respectively) but from an even more dramatic *contrast enhancement* due to being stretched out from underneath the unresolved quasar by the magnification. We discuss some of these issues

further in the Appendices.

2.2. Estimating The Rest-Frame R -Band Luminosities of Host Galaxies

To proceed further, we use the H -band flux measurements to estimate the rest-frame R -band luminosities of the host galaxy bulges presented in Tables 3 and 4. Fig. 7 shows the conversion between H -band and rest-frame R -band as a function of redshift for galaxies with different spectral types from Coleman, Wu & Weedman (1980).¹¹ Since the H -band roughly corresponds to the rest frame R -band at $z \sim 1.4$ the conversions are only weakly dependent on the assumed SED for the redshift range $1 \lesssim z \lesssim 2.5$. For example, at $z = 2$ the spread between doing the conversion with the reddest (E/S0) and bluest (Im) SEDs is only 0.3 mag (Figure 7). At higher redshifts, the choice of SED becomes very important, and by $z \sim 4.5$ the magnitude difference varies by 2.5 mag between the E/S0 and Im SED models. We adopt the Sbc template as our standard model. The Sbc template predicts an $I - K$ color of $\simeq 3$ AB mag that is typical of a distant, $z \gtrsim 2$ red galaxy (Labbé et al. 2005). It is 1–2 mag redder than typical Lyman break galaxies, which are better modeled by the Im SED. While we adopt the Sbc model as our standard model, we will explore the consequences of the extreme assumptions of an E/S0 or Im SED on our results.

One extreme alternative to using a $z = 0$ Sbc SED for the k -correction template is to use that of an Ultra-Luminous Infrared Galaxy (ULIRG) because the high levels of star formation and dust obscuration in a ULIRG may be more representative of quasar host galaxies than a nearby normal galaxy. As shown in Fig. 7 the k -corrections derived from the Devriendt, Guiderdoni, & Sadat (1999) SED for the nearby, prototypical ULIRG Arp 220 are midway between those of the Sbc and Scd templates at all relevant redshifts. Thus, our estimated restframe luminosities are insensitive to whether we treat the host as a normal galaxy or a ULIRG.

Since the lensed quasar and host images pass near or through the lensing galaxy, some extinction may be caused by the lensing galaxy. Typical lens galaxies produce differential extinction of lensed quasars with a median $\Delta E(B - V) \simeq 0.08$ mag (Falco et al. 1999). For a standard $R_V = 3.1$ extinction law this would lead to a correction to the host luminosity (assuming a uniform dust screen) of only $A_H \simeq 0.05$ mag for a lens at $z = 1$, with smaller corrections at lower lens redshifts. There is considerable evidence that the lens galaxies show a range of extinction curves (e.g. Falco et al. 1999, Muñoz et al. 2004), but these variations occur at wavelengths $\lesssim 4000$ Å rather than the rest-frame near-IR or optical wavelengths that we use. There are some lenses with significantly higher extinction (in B1608+656 differential extinction of the host galaxy is observed – Koopmans et al. 2003; Surpi & Blandford 2003), but we have not included any of these systems in our analysis. In short, we make no corrections for extinction of the host galaxy

¹¹ We follow Hogg et al. (2004) in computing detailed k -corrections. We transform the HST Vega-based magnitudes to R -band using the Coleman, Wu, & Weedman (1980) templates and appropriate filter transmission curves. The integrated fluxes are normalized to a spectrum of α -Lyr, “observed” in the appropriate bandpass.

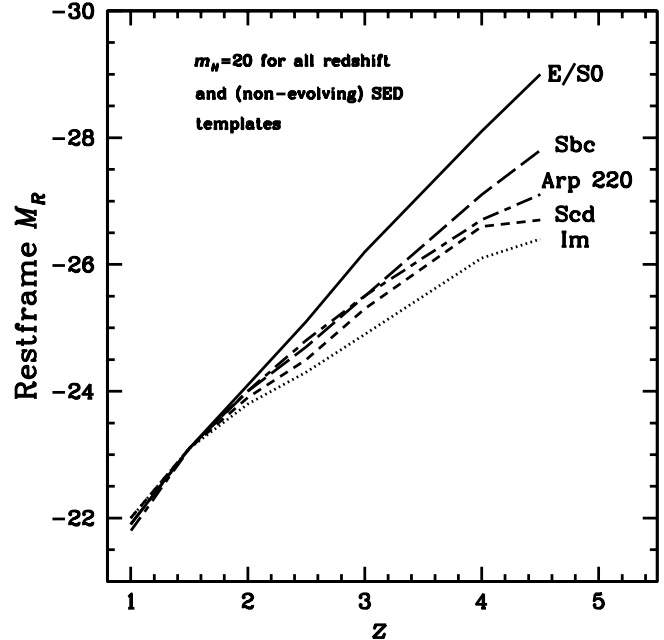


FIG. 7.— The absolute, restframe R -band luminosity for a galaxy with an observed H -band luminosity of 20 mag for four different models of the SED. The SEDs are the E/S0, Sbc, Scd, and Im models from Coleman, Wu, & Weedman (1980). Note that for our redshift range, all SEDs bluer than the E/S0 model have fainter restframe luminosities than the estimate from the E/S0 model.

by dust in the lens galaxy because they are likely to be small.

3. VIRIAL BLACK HOLE MASS ESTIMATE

We estimate \mathcal{M}_{BH} using the virial technique applied to the C IV ($\lambda 1549$ Å), Mg II ($\lambda 2798$ Å), and the H β ($\lambda 4861$ Å) emission line widths and their local continuum luminosities $\lambda L_{\lambda}(1300$ Å), $\lambda L_{\lambda}(3000$ Å) and $\lambda L_{\lambda}(5100$ Å) respectively. We adopt the normalization of Onken et al. (2004), confirmed through a much larger sample by Greene & Ho (2005), between the virial relations to local measurements of black hole masses. This normalization is a factor of 1.8 higher than earlier normalizations. Combining the BLR radius estimates of Kaspi et al. (2005) and the new normalization factor, we adopt virial relations of

$$\mathcal{M}_{\text{BH}} = A_{\text{line}} \left[\frac{\text{FWHM}(\text{line})}{1000 \text{ km s}^{-1}} \right]^2 \left[\frac{\lambda L_{\lambda}(\lambda_{\text{line}})}{10^{44} \text{ erg s}^{-1}} \right]^{\gamma_{\text{line}}} \mathcal{M}_{\odot}, \quad (4)$$

with $\lambda_{\text{line}}\{\text{CIV}, \text{Mg II}, \text{H}\beta\} = \{1350, 3000, 5100\}$ Å, $A_{\text{line}}\{\text{CIV}, \text{Mg II}, \text{H}\beta\} = \{4.5, 6.1, 5.9\} \times 10^6$, and $\gamma_{\text{line}}\{\text{CIV}, \text{Mg II}, \text{H}\beta\} = \{0.53, 0.47, 0.69\}$ (Vestergaard & Peterson 2006, McLure & Jarvis 2002, Kaspi et al. 2005, respectively). We refer the reader to P06 and references therein for a detailed discussion of the method and its limitations.

Tables 3 and 4 summarize our estimates of the quantities needed to estimate \mathcal{M}_{BH} , as well as our final estimate of \mathcal{M}_{BH} for those objects which have published spectra. For the lensed quasars we estimated the FWHM by manually estimating the FWHM from paper copies of published spectra; two of the authors independently es-

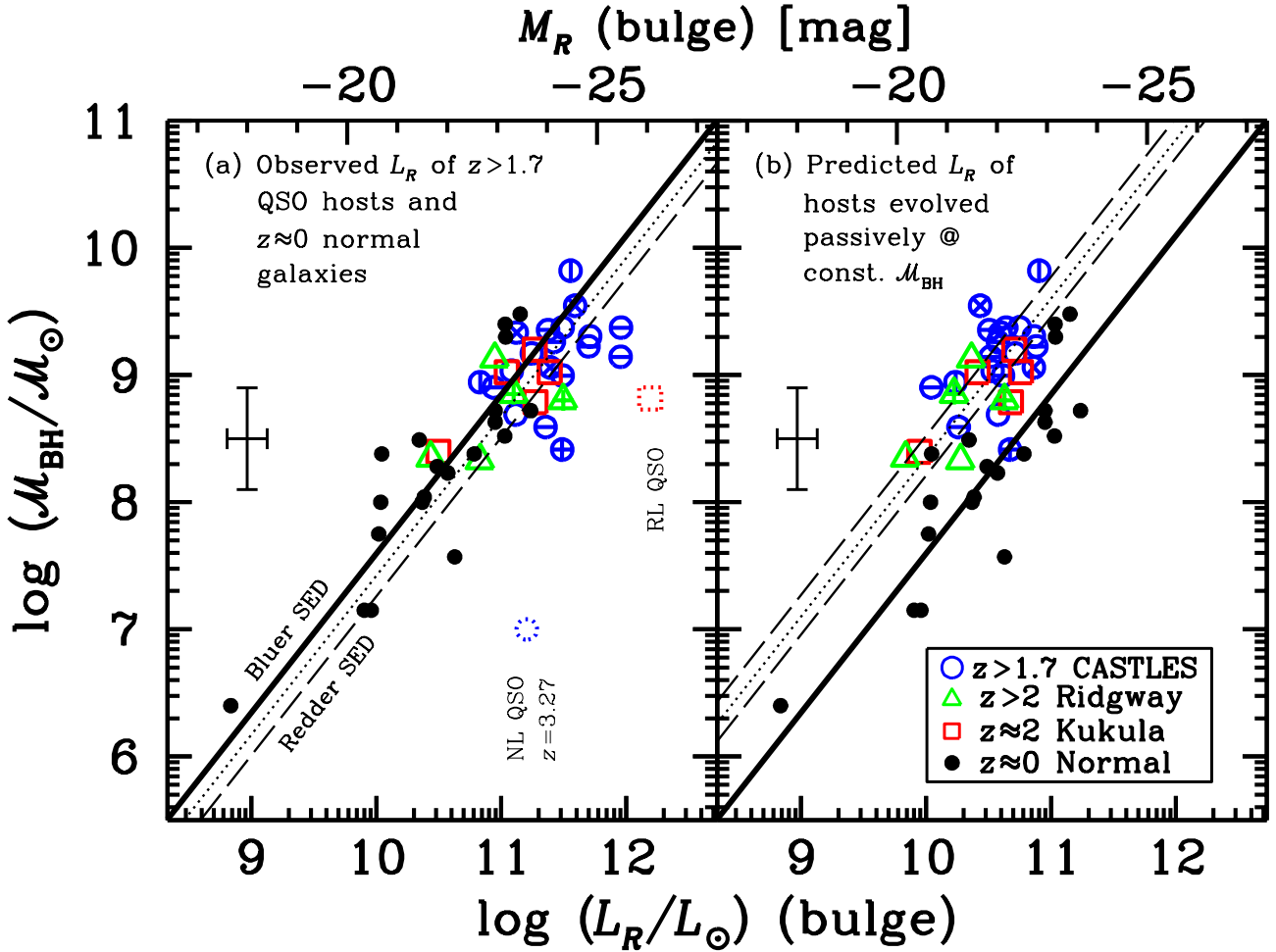


FIG. 8.— The observed (a, left) and evolution corrected (b, right) correlations between black hole mass and host luminosity for the high redshift host sample. The round solid points are the local comparison sample, and the solid line is the best fit, local relationship between \mathcal{M}_{BH} and host luminosity. The high redshift hosts are shown using circles for the gravitationally lensed hosts, triangles for the Ridgway et al. (2001) hosts and squares for the Kukula et al. (2001) hosts. An Sbc SED was used to make all the k -corrections. The dotted line shows the best fit relation for the high redshift hosts using the Sbc SED to make the k -corrections, and the dashed lines show the effect of using either the E/S0 (redder SED) or Im (bluer SED) templates rather than the Sbc template. Points with vertical lines (!) show broad absorption features in their spectra which may make the estimate of \mathcal{M}_{BH} a lower limit. Points with horizontal lines have $z > 2.5$. The point that is crossed out is not included in the fits (see Appendix). The dotted lines fitted to the $z \approx 2$ (open) points are displaced from the $z = 0$ relationship by 0.3 (a) and 1.5 (b) mag. The dotted circle and square illustrate problematic objects which are discussed in the text and in Appendix D. These two objects are excluded from further discussions. In the representative errorbar shown, the \mathcal{M}_{BH} error is the scatter in the virial relation, while the host galaxies have an uncertainty of roughly 0.3 mag.

estimated the widths, finding consistency. The AGN continuum luminosity comes from first separating the AGN from the host galaxy in the lens image fitting as described above. We then fit this broad-band *HST* photometry (V , I and H) with a power law to estimate the continuum luminosities entering the virial relations. Since the virial relations depend only on the (roughly) square root of the continuum luminosity, even substantial errors have little effect on the estimate of \mathcal{M}_{BH} . The corresponding values shown in Table 4 for the Ridgway et al. (2001) and Kukula et al. (2001) samples are from P06 after changing from the E/S0 template (P06) to the Sbc template (here) used for making k -corrections to the host galaxy photometry. For seven of the QSOs we can estimate \mathcal{M}_{BH} from both the C IV and Mg II. Four of 9 agree to better than 30% while the other five differ by factors of 0.5, 0.5, 1.5, 3, and 3. The agreement is reassuring and consistent with other studies finding that the

virial technique mass estimates have a scatter of a factor of ~ 3 (Kaspi et al. 2000, Vestergaard 2002, McLure & Jarvis 2002, Kollmeier et al. 2005). For the 9 objects with multiple \mathcal{M}_{BH} estimates we adopt the average.

4. RESULTS

We examine the evolution of the $\mathcal{M}_{\text{BH}}-L_R$ relationship by dividing our host sample into two sub-samples which span equal time intervals and comparing them to the local relation. Our high redshift sub-sample of 31 objects spans the period 10–12 Gyrs ago ($1.7 \lesssim z \lesssim 4.5$) and our low redshift sub-sample of 20 objects spans the period 8–10 Gyrs ago ($1.0 \lesssim z \lesssim 1.7$). We use the sample of 20 nearby, normal early-type galaxies, excluding lenticular galaxies, with \mathcal{M}_{BH} measurements by Kormendy & Gebhardt (2001) and L_R measurements from Bettoni et al. (2003). The $\mathcal{M}_{\text{BH}}-L_R$ relation for these local galaxies is

well fitted by a power law

$$\log(\mathcal{M}_{\text{BH}}/\mathcal{M}_{\odot}) = -0.50(\pm 0.06)M_R - 2.70(\pm 1.35), \quad (5)$$

where we have converted the original Bettoni et al. (2003) result to our standard cosmological model. Most of the individual local objects fall within 0.5 mag of this relation, as do nearby radio galaxies (Bettoni et al. 2003) and local quasar and Seyfert hosts (McLure & Dunlop 2002).

Figs. 8 and 9 compare the high and low redshift samples to the local sample both as observed and with evolutionary corrections. In addition to marking the origin of the hosts (filled circles for the local comparison sample, open circles for the lensed hosts, triangles for the Ridgway et al. (2001) hosts and squares for the Kukula et al. (2001) hosts), we have also flagged objects with additional complications. The 8 systems marked with a vertical bar (|) have absorption features near their broad emission lines which might lead to an underestimate of the line width and hence the black hole mass. Objects at $z > 2.5$ are marked with a horizontal bar (—) because their luminosities are much more sensitive to the choice of an SED to make the k -corrections. Finally, there are four objects discussed in the Appendix D, marked either by a diagonal-cross (×) or shown in dotted lines, that may be problematic. We do not include them in the subsequent analysis. The representative errorbars for the gravitational lenses are also shown in the Figures, where the uncertainty in the \mathcal{M}_{BH} (Y -direction) is represented by the scatter in the virial technique. Whereas, for the host galaxies (X -direction), typical uncertainties are roughly 0.3 magnitude for the gravitational lenses. For non-lenses, typical errorbars on the host luminosities are roughly 0.5-0.8 mag (Ridgway et al. 2001, Kukula et al. 2001).

4.1. The Evolution of the $\mathcal{M}_{\text{BH}}\text{-}L_R$ Relation Since $1.7 \lesssim z \lesssim 4.5$

We first consider the $\mathcal{M}_{\text{BH}}\text{-}L_R$ relation of the high redshift sample ($z \gtrsim 1.7$) illustrated in Fig. 8a. The observed relation at these redshifts is nearly identical to the local relation – if we fit the high redshift sub-sample using Eqn. 5 with the slope fixed, then the shift is only 0.3 mag in L_R or 0.2 dex in \mathcal{M}_{BH} , with an RMS scatter of 0.4 dex in \mathcal{M}_{BH} , and 0.8 mag in M_R around the best fitting line. This confirms the results of P06, but with three times as many data points. The data show that host galaxies harboring black holes of the same mass \mathcal{M}_{BH} were as luminous in the R -band at $z \gtrsim 1.7$ as they are now, despite the passage of 10 Gyrs.

Physically, we are interested in the relative growth rates of the black hole and its host, which we can characterize by the black hole mass per unit stellar mass, $\mathcal{M}_{\text{BH}}/\mathcal{M}_{*}$. This is related to the observed luminosity by the mass-to-light ratio of the stellar population, \mathcal{M}/L . We will measure the evolution of the black hole and the hosts by looking for changes in the specific stellar mass $\mathcal{M}_{\text{BH}}/\mathcal{M}_{*}$ with redshift, which we can quantify by the stellar mass deficit between the observed host and a bulge on the present day $\mathcal{M}_{\text{BH}}\text{-}\mathcal{M}_{*}$ relation,

$$\begin{aligned} \Gamma(z) &= \frac{\mathcal{M}_{*}(\text{local bulge})}{\mathcal{M}_{\text{BH}}} \frac{\mathcal{M}_{\text{BH}}}{\mathcal{M}_{*}(\text{host at } z)} \\ &= \frac{L_R(\text{local bulge})}{L_R(\text{host at } z)} \times \frac{\mathcal{M}/L(\text{local bulge})}{\mathcal{M}/L(\text{host at } z)} \end{aligned}$$

$$= \frac{L_R(\text{local bulge})}{L_R(\text{host evolved to } z=0)}$$

where the last conversion holds because the luminosity of the stars in the host will have at redshift zero is simply the observed luminosity multiplied by the ratio of the initial and final mass-to-light ratios. The magnitude of the mass deficit determines the amount by which the stellar mass of the host must grow for the system to reach the present day $\mathcal{M}_{\text{BH}}\text{-}\mathcal{M}_{*}$ relation. We want to consider evolutionary corrections that are conservative in the sense that any other choice will increase the stellar mass deficit. This means that we will underestimate the required evolution in $\Gamma(z)$, or equivalently, that we underestimate the growth in the stellar mass that must occur in the host between its redshift and the present day due to star formation and mergers.

For normal stellar populations, the most conservative model is to assume that all the stars in the host were formed at some much higher redshift (we adopt $z_f = 5$) and then evolve passively to the present epoch. If the mean formation redshift of the stars is lower than this redshift, then the stellar population has a lower mass-to-light ratio than in the model, so we will overestimate the mass-to-light ratio of the observed host, underestimate the amount by which the mass-to-light ratio will evolve, and hence underestimate the mass deficit $\Gamma(z)$. Adopting a higher formation redshift has little effect since the fading rate only changes from $dM_R/dz \simeq -0.8$ mag for $z_f = 5$ to $dM_R/dz \simeq -0.6$ mag for $z_f \rightarrow \infty$ in the Bruzual & Charlot (2003) population synthesis models, with solar metallicity, Salpeter IMF, and no reddening (van Dokkum & Franx 2001). Higher formation redshifts will modestly reduce the stellar mass deficit, but it is a small correction even for unphysically high mean star formation epochs. We adopt this passively evolving model for our standard evolutionary corrections in estimating the stellar mass deficit and find that the mass deficit is a factor of ~ 4 at $z \gtrsim 1.7$.

One problem could invalidate our belief that our estimate of the mass deficit is a lower bound, and that is the presence of significant dust extinction in the host galaxy. If fraction $f \leq 1$ of the stellar light is absorbed by dust, then we have overestimated the stellar mass deficit by the same factor. The problem, however, is that the net effect of the presence of dust on the mass-to-light ratio is complex because higher levels of extinction are generally associated with smaller intrinsic mass-to-light ratios due to higher levels of star formation. In local ULIRGs, the extra luminosity from young stars generally prevails over dust extinction and the ULIRG has a lower mass-to-light ratio than a passively evolving stellar population (Lonsdale, Farrah & Smith 2006). For example, Arp 220 has a mass-to-light ratio of approximately $\mathcal{M}/L \simeq 2$ based on estimates of the stellar velocity dispersion from Doyon et al. (2004), and this is only 50% that of a nearby early-type galaxy (e.g. Cappellari et al. 2005). Thus, if Arp 220 is representative of a typical host galaxy, the stellar mass deficit would be $\Gamma \simeq 2$. On the other hand, most $z \simeq 2$ galaxies have $\mathcal{M}/L_R \simeq 0.5$, and only the reddest galaxies reach $\mathcal{M}/L_R \simeq 2$ whether due to dust or age (Shapley et al. 2005). It is difficult to determine whether local ULIRGs are good analogies for high redshift hosts, but it is still likely that there is a significant

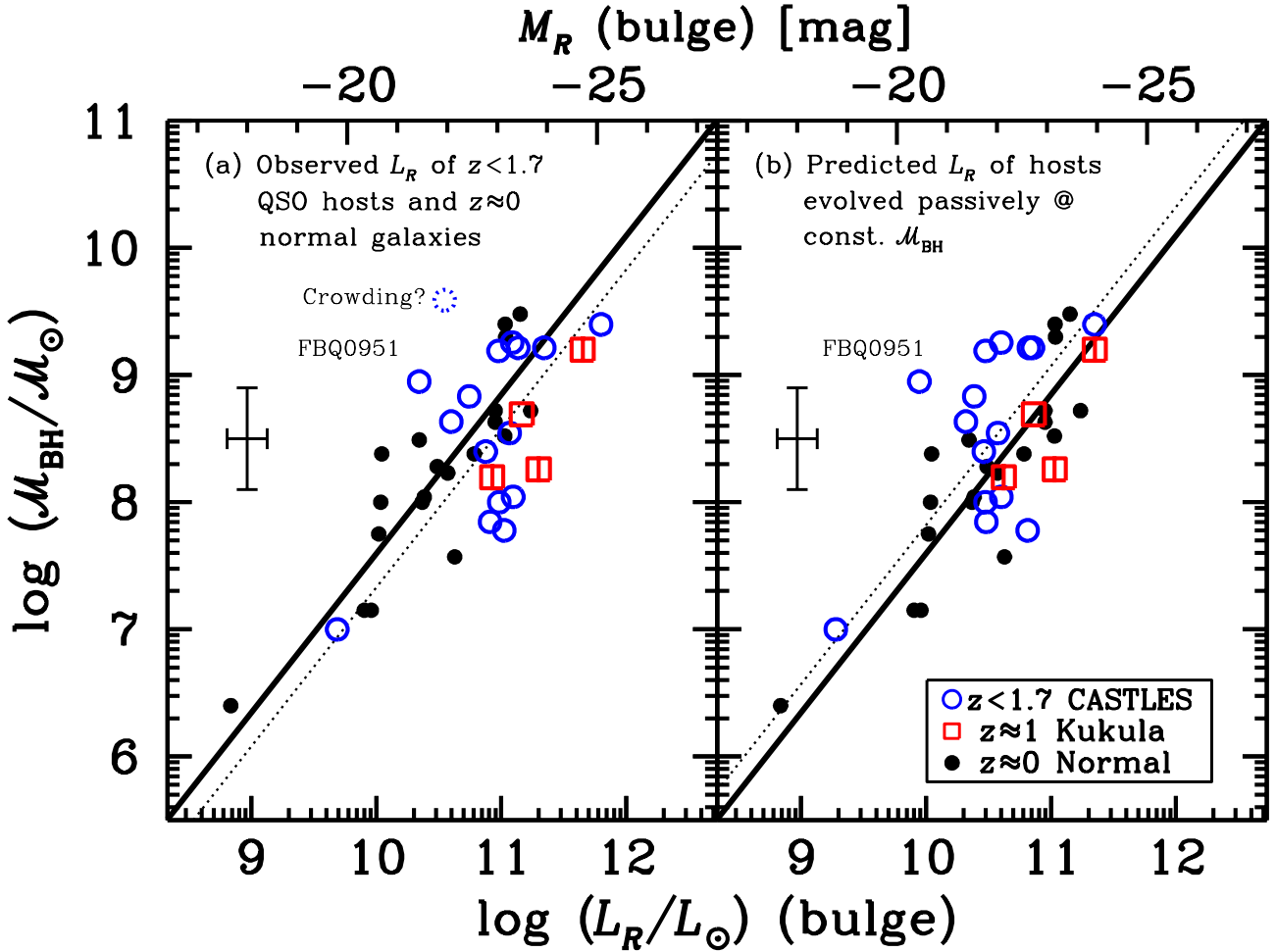


FIG. 9.— The observed (a, left) and evolution corrected (b, right) correlations between black hole mass and host luminosity for the lower redshift ($z \lesssim 1.7$) host sample. See Figure 8 for details. Points with a vertical line (!) may have underestimated values of \mathcal{M}_{BH} due to either broad absorption features or narrow emission line components. The dotted line is displaced from the solid line representing the local $\mathcal{M}_{\text{BH}}-L_R$ relation by 0.5 magnitude. See Appendix regarding FBQ 09051+532.

stellar mass deficit under the hypothesis that the quasar hosts are dusty, star forming galaxies.

In summary, our overall estimate is that the stellar host for a black hole of fixed mass at $z \gtrsim 1.7$ is on average a factor of 4 less massive than today if we use the Sbc model for the k -corrections. Leaving out $z \gtrsim 3$ object lowers the deficit by $\lesssim 10\%$. The mass deficit rises to a factor of 6 for the Im SED and falls to a factor of 3 for the E/S0 SED, so we adopt 4_{-1}^{+2} as our standard estimate. This estimate of the deficit is designed to be a lower bound in the sense that any other assumption about the stellar populations in the host corresponds to adding more rapidly evolving, younger stellar populations that will increase the correction for evolution and thus increase the mass deficit compared to a passively evolving model. If all the scatter were due to random effects, this is a 6σ result, given an RMS scatter of 0.4 dex in \mathcal{M}_{BH} and 0.8 mag in M_R .

4.2. The Evolution of the $\mathcal{M}_{\text{BH}}-L_R$ Relation Since $1 \lesssim z \lesssim 1.7$

When we carry out the same analysis for our low redshift sample, as shown in Fig. 9, we find that the

host galaxy mass deficit (Fig. 9b) is at most a factor of two. The observed R -band luminosities are about 0.5 mag brighter than the local relation, but the passive evolution-corrected luminosities are about 0.5 mag fainter than the local relation. Unfortunately, we have fewer points and they exhibit more scatter (0.7 dex in \mathcal{M}_{BH} , 1.2 mag in M_R) than we found for the higher redshift sample.

The larger scatter is due to several factors. First, we have fewer objects in this redshift bin and several of them may be problematic (see the Appendix D). One lensed host, SBS 0909+532 ($z = 1.38$) we discard entirely because the fits are unstable. Another lensed host, FBQ 0951+2635 ($z = 1.24$) is well-detected and modeled, but lies 3 mag from the general trend. We include it in the fits since we lack an objective basis for rejecting it, but it does bias our fits towards fainter hosts by 0.15 mag and accounts for a third of the implied evolution of this redshift bin. Six of the unlensed hosts may have biased estimates of the black hole mass due to beaming effects, contributions from narrow emission lines or broad absorption lines (see Appendix A). As a second source of scatter, the stellar populations in this redshift range may be more heterogeneous simply because the

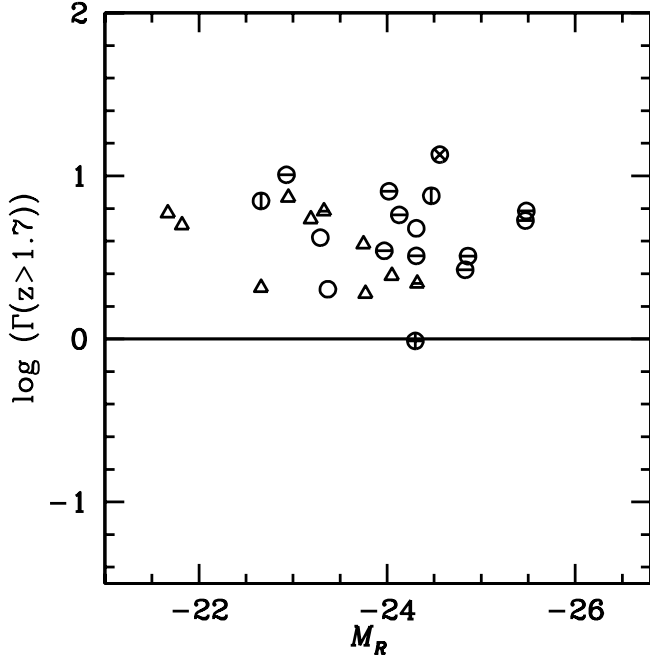


FIG. 10.— The $\mathcal{M}_{\text{BH}}/\mathcal{M}_*$ ratio Γ (relative to $z = 0$) as a function of rest-frame R -band luminosity M_R for galaxies between look-back times of 10 and 12 Gyr ($1.7 \lesssim z \lesssim 4.5$). The circles are the lensed hosts and the triangles are the directly imaged hosts from Ridgway et al. (2001) and Kukula et al. (2001). Points with $z \geq 2.5$ have a horizontal line through the symbol (see Table 2), and points with a vertical line may represent lower limits because \mathcal{M}_{BH} may be underestimated due to narrow line contamination or broad absorption features in the spectra we used to estimate \mathcal{M}_{BH} . Only one host, B 1422+231 (marked by \times) is a possible non-detection, so Malmquist bias is unimportant.

universe is older. In our high redshift bin, all stars must be < 3 Gyr old (at $z = 2$), while in this bin they can be up to 6 Gyr old. An increasing diversity in the average age of the stellar populations will appear as scatter. A third point is that the hosts seem to make up much of the stellar mass deficit we observed for the high redshift hosts in this lower redshift range, leading to a systematic offset between the high- and low-redshift object ends of the $1 \lesssim z \lesssim 1.7$ range.

Thus, we conclude that the $\mathcal{M}_{\text{BH}}-L_R$ relation also existed 8–10 Gyr ago, but with a significantly smaller offset from the local relation than we observed in the higher redshift sample, and with a larger RMS scatter (0.7 dex in \mathcal{M}_{BH} , 1.2 mag in M_R). Unfortunately, with the small numbers of objects and the increased scatter among them, it is difficult to quantify this qualitative trend precisely. At most, a stellar mass deficit of a factor of two is permitted, but the statistical significance appears weak ($\sim 1\sigma$). Thus the host galaxies could be consistent with being passively evolving since $z \sim 1$.

5. DISCUSSION AND CONCLUSION

Figs. 10 and 11 summarize the results by showing the stellar mass deficit $\Gamma(z)$ of the hosts as a function of luminosity and redshift. Figure 11 is equivalent to the evolution of the $\mathcal{M}_{\text{BH}}/\mathcal{M}_*$ ratio. While we see little correlation of $\Gamma(z)$ with luminosity (Fig. 10), we see considerable evidence for a correlation with redshift and look-back time (Fig. 11). A detailed study of the evolution with redshift is now limited by small number statistics at

$z \gtrsim 3$ and $z \lesssim 1.5$. Crudely it appears that $\Gamma(z)$ evolves little to $z \sim 1$, rises to $\Gamma(z) \sim 4$ at $z \sim 2$ and then saturates at a factor of ≈ 6 . If we assumed a bluer SED for the $z > 1.7$ sample, the rising trend would continue further, while if we assumed a redder SED, it would decline at the higher redshifts (Fig. 11). We will address this issue in more detail as we acquire color information for the hosts.

If real, this trend must arise from a combination of on-going star formation and mergers between galaxies. Star formation provides a very simple explanation, particularly since the evolution of $\Gamma(z)$ looks remarkably similar to estimates of the star formation history in which the rates are roughly constant to $z \sim 1$ and then decline rapidly, with at least 50% of the stellar mass in place by redshift unity (e.g. Bauer et al. 2005 or Feulner et al. 2005).

A simple way to parameterize the amount of star formation needed to achieve agreement with normal galaxies today is through estimating the required amount of specific star formation, ϕ , the SFR per unit mass. Thus, a quasar host with mass deficit Γ would require an average star formation rate of $\langle \phi \rangle = (\Gamma - 1)/\Delta t$ [Gyr^{-1}], if all the missing stellar mass forms in the time span of Δt . Our estimated mass deficit of $\Gamma = 4$ between $z = 2$ and $z = 1$ ($\Delta t = 2.5$ Gyrs) leads to $\langle \phi \rangle = 1.2 \text{ Gyr}^{-1}$. Such a star formation rate, though high for the most massive objects in our study, is in fact observed in $z \sim 2$ galaxies (Reddy et al. 2006), which would also require quasar hosts at $z \sim 2$ to be very actively star forming. However, if not all the mass deficit is fully accounted for by $z \approx 1$, as possibly our data suggest, then the star formation rate needed can be as low as $\langle \phi \rangle = 0.6 \text{ Gyr}^{-1}$, which is seen in some distant red galaxies (Reddy et al. 2006). The typical star formation in a Lyman break galaxy of $\phi \gtrsim 2$ (Reddy et al. 2006; Ouchi et al. 2004; Reddy, Steidel, & Erb 2005) is more than sufficient to eliminate the stellar mass deficit of the bulge hosting a $10^8 \mathcal{M}_\odot$ BH. By adding a modest amount of internal extinction or extending the period of star formation, the required SFR could be even lower. The rest-frame UV colors of hosts at high redshifts tend to be fairly blue and are consistent with on-going star formation (Jahnke et al. 2005). On the other hand, if the central BHs gain significantly in mass over this time through accretion, as opposed to BH merging, then the required star formation rate would have to rise proportionally.

Many massive galaxies will also experience major mergers over this redshift range, which can also lead to evolution in $\Gamma(z)$. Mergers of pure bulge galaxies can only move systems along the $\mathcal{M}_{\text{BH}}-L_R$ relation, but major mergers of systems with disks increase $\Gamma(z)$ as the disks are disrupted and added to the bulge. A merger of two identical galaxies with a bulge-to-disk ratio of (B/D) reduces $\Gamma(z)$ by a factor of $1 + (B/D)^{-1}$, if all the disk stars are incorporated into the bulge. The process can reduce $\Gamma(z)$ by large factors only if the hosts are disk-dominated systems, which currently cannot be constrained given our relatively shallow exposures. Detailed studies of the highest signal-to-noise objects will be discussed in Peng et al. (2006 in preparation). Mergers with smaller satellites would contribute to decreasing $\Gamma(z)$ but not by large factors. Thus, mergers prob-

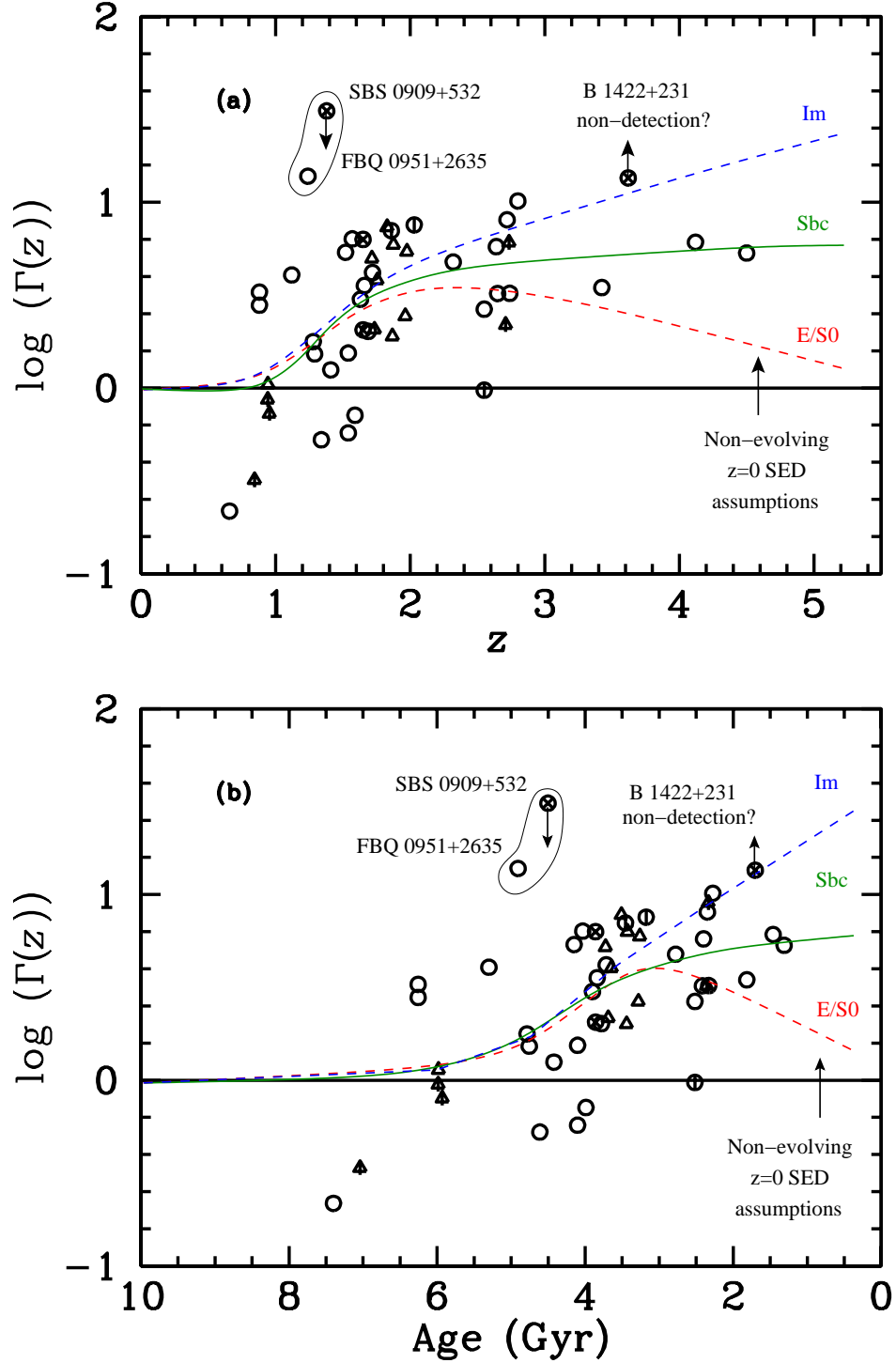


FIG. 11.— The $\mathcal{M}_{\text{BH}}/\mathcal{M}_*$ ratio Γ normalized to $z=0$, or equivalently the host mass deficit, as a function of redshift (Panel *a*) and time (Panel *b*). The symbols are the same as in Figure 10. The curves roughly indicate the consequences of using different non-evolving, $z=0$, SED templates to compute the k -corrections. All data points are based on assuming the Sbc SED (solid line) as in Fig. 8. All the scenarios assume the same passive-evolution corrections. Changing to any more rapidly evolving model would increase the $\mathcal{M}_{\text{BH}}/\mathcal{M}_*(z)$ ratio.

ably contribute to the downward evolution of $\Gamma(z)$ but may not dominate the evolution. On the other hand, it has been suggested that if the BH masses were to grow by $\gtrsim 10\times$ since $z \approx 2$, and the local $\mathcal{M}_{\text{BH}}\text{-}L_{\text{bulge}}$ relation were to greatly *steepen* for $\mathcal{M}_{\text{BH}} \gtrsim 3 \times 10^9 M_{\odot}$, the amount of galaxy mass growth required can be less than our inference. However, this appears not to be an issue, given a recent work which extends the local $\mathcal{M}_{\text{BH}}\text{-}L_{\text{bulge}}$ relation to some of the largest BH masses (Lauer et al. 2006, in preparation).

Improving our results depends on obtaining three new types of data. First, we need to quantify the color and structure of the host galaxies to better understand their structures and stellar populations. In our structural study of the hosts (Peng et al. 2006, in preparation), we find that the typical hosts have effective radii of $r_e \lesssim 3\text{-}5$ kpc that are significantly smaller than present-day galaxies with the same \mathcal{M}_{BH} , and that they may be less concentrated. As mentioned earlier, the hosts seem to have fairly blue rest-frame UV colors that imply star formation rates of order $\sim 20 M_{\odot} \text{ yr}^{-1}$ (Jahnke et al. 2005). Second, we need to increase the number of hosts with measured properties, particularly in the redshift range $0.5 < z < 2.0$, to better probe the evolution of $\Gamma(z)$ and to begin studying the evolution of the dispersion of the $\mathcal{M}_{\text{BH}}\text{-}L_R$ relation with redshift. Third, it would be a very useful check of the virial relations if the sizes of the broad line emitting regions of quasars at $z > 1$ could be measured directly as a check for evolution in the relations. While reverberation mapping methods probably cannot be used due to the time scales, it is likely that gravitational lensing can be used to make the measurements by examining the microlensing of the broad line region by stars in the lens galaxy. There is considerable evidence now that the continuum and emission line regions are differentially microlensed (e.g. Wayth, O’Dowd

& Webster 2005; Popović et al. 2006), and the next challenge is to use these differences to estimate the sizes of the regions (Richards et al. 2004; Keeton et al. 2005). This has been done for the continuum regions of several lensed quasars, the $z = 1.7$ quasar Q 2237+0305 in particular (see Kochanek, Schneider, Wambsganss 2004 and references therein).

We thank Sandy Faber, Marianne Vestergaard and Xiaohui Fan, Tod Lauer, Luis Ho, Jenny Greene, Mike Santos, and Roeland van der Marel for enlightening discussions on various issues of the black hole/galaxy correlation, and John Moustakas for discussions on k -correction issues. We also thank the anonymous referee for a thoughtful report. The work of CYP was performed in part under contract with the Jet Propulsion Laboratory (JPL) funded by NASA through the Michelson Fellowship Program. JPL is managed for NASA by the California Institute of Technology. CYP is also grateful to STScI for support through the Institute Fellowship Program. We also thank the SDSS collaboration for providing such a valuable database. Support for the CASTLES project was provided by NASA through grant numbers GO-7338, GO-7495, GO-7887, GO-8175, GO-8252, GO-8804, GO-9133, GO-9138, GO-9375, and GO-9744, from the Space Telescope Science Institute, which is operated by the Association of Universities for Research in Astronomy, Inc., for NASA, under contract NAS5-26555. Our research was also supported by the Smithsonian Institution. This research has made use of the NASA/IPAC Extragalactic Database (NED) which is operated by the Jet Propulsion Laboratory, California Institute of Technology, under contract with the National Aeronautics and Space Administration.

APPENDIX

SYSTEMATIC ERRORS DUE TO MALMQUIST BIAS AND ASTROPHYSICAL ASSUMPTIONS

Peng et al. (2005) discussed the known sources of systematic and random uncertainties in the $\mathcal{M}_{\text{BH}}\text{-}L_R$ and the $\mathcal{M}_{\text{BH}}\text{-}\mathcal{M}_{\star}$ relations in detail, but it is worth reviewing the major concerns. We have already discussed our conservative approach to correcting and evolving the SED of the host galaxy and a dusty starburst scenario (§ 2.2), where by conservative we mean that alternative choices would lead to larger estimates of the evolution in $\mathcal{M}_{\text{BH}}/\mathcal{M}_{\star}$ than we report. Other issues that could affect the results are Malmquist biases, PSF model problems, and the applicability of the local virial relations to high redshift systems.

Malmquist bias, where we detect only the most luminous hosts, can matter little because our sample is nearly complete. There is only one system out of 51 for which we are uncertain about the host detection. Moreover, the effect of missing lower luminosity hosts would only increase the necessary amount of evolution because it would mean that the actual mean host luminosity is fainter than our estimates. Reducing our estimate of the evolution in $\mathcal{M}_{\text{BH}}/\mathcal{M}_{\star}$ means that we must be *under-estimating* the host galaxy luminosities by 1.5 mag, *over-estimating* the black hole masses by 0.6 dex (a factor of 4), or some combination of both effects. It is possible for the host luminosities to be underestimated by 0.2-0.3 magnitudes due to either problems in the PSF models (Sánchez et al. 2004) or limits to our surface brightness sensitivity, but this effect is much smaller for lensed than for unlensed hosts.

P06 demonstrated that the systematic errors due to the PSF model for the Kukulka et al. (2001) and Ridgway et al. (2001) samples are small compared to the observed evolutionary trends. In Appendix C we present results for comparing the fits to long and short exposures of the same lensed object, also finding no significant biases. Moreover, our sample of lensed hosts is less sensitive to this problem than traditional samples of high redshift host galaxies. This reduction in systematic uncertainties is not offset by the need to model the lensing effects. As we discuss in the Appendices B, the lens model introduces no significant biases unless we assume that galaxies have no dark matter halos – an assumption leading to a host of other cosmological complications. Finally, we note that the agreement of the estimated properties of lensed and unlensed host galaxies suggests that neither has major systematic problems.

The conclusions in this study are sensitive to systematic shifts between the local virial calibrations for \mathcal{M}_{BH} and higher redshifts. There is no theoretical mechanism for such changes because the virial relation should depend only on

the local accretion physics of black holes. Netzer (2003), Vestergaard (2004) and Baskin & Laor (2005) discuss why they should be applicable to luminous quasars and the potential caveats. In fact, Baskin & Laor (2005) found that for C IV lines wider than 4000 km s^{-1} , as for most objects here, the virial BH mass estimator may actually be biased towards *low* \mathcal{M}_{BH} estimates, and such a correction would increase the estimated evolution. Internal to our sample we see no systematic offsets in the \mathcal{M}_{BH} estimates from the Mg II and C IV for the 6 objects with both lines. A much larger study by Kollmeier et al. (2005) also finds consistent results from different lines, and considerable evidence that there can be little systematic scatter in the \mathcal{M}_{BH} estimates for quasars of comparable redshift and luminosity.

Lastly, as discussed in Section 2.2, a dusty starburst of the type like Arp 220 has a bluer SED and a lower \mathcal{M}/L ratio than a local stellar bulge. Moreover, even without the compensating effects of a reduced \mathcal{M}/L ratio, and the fact that dust is included *implicitly* in our choice of SED templates, it would take an additional 1.5 mag of R -band extinction to weaken our conclusions. This level of *absolute* extinction is more typical of the extinction for Lyman break galaxy in the restframe ultraviolet (1600 \AA , Shapley et al. 2001) than our restframe optical measurements (H -band is still only 2900 \AA in the rest frame of our highest redshift host, at $z = 4.5$). In summary, the net effect of a dusty star burst having a lower \mathcal{M}/L ratio than our SED assumptions would imply a *larger* amount of evolution in the $\mathcal{M}_{\text{BH}}/\mathcal{M}_*$ ratio than redder, passively evolving, host galaxies.

LENS MODEL DEGENERACIES

The complexities of the lens modeling process coupled with image fitting are often causes of concern to non-practitioners even if they are well understood by the practitioners. Here we briefly discuss some of the most common concerns. Readers interested in a detailed review of lens models and their limitations should see Kochanek, Schneider, & Wambsganss (2004).

Gravitational lenses are extraordinarily good at constraining the angular structure of the gravitational potential, particularly when the host galaxy forms a well-defined Einstein ring around the lens (e.g. Fig. 3). Analyses of these rings show that the gravitational potentials are centered on the luminous lens galaxies and that the deviations of the potential from that of an ellipsoid are consistent with zero (Yoo et al. 2005). This means that the only real freedom in our model is adjusting the radial density profile of the lens, which corresponds to adjusting the mass of the dark matter halo of the lens relative to the visible galaxy.

For many lensing galaxies, the observations cannot determine the exact radial density profile because of the mass sheet degeneracy. An example of this degeneracy is the fact that most of our lensing galaxies reside inside a weak galaxy cluster which acts like a uniform mass sheet at the scale of the lensed images that causes an additional, isotropic, magnification. If we take a lens and add a constant surface density sheet, κ in units of the critical density for lensing, then the only observable quantity that is altered is the time delay between the images. The effect on the properties of the host are a simple magnification – if additional surface density is added, then the scale length of the host shrinks by factor of $(1 - \kappa)$ and its flux drops by a factor of $(1 - \kappa)^2$. The effect of changing the density profile of the lensing galaxy itself is a local analog of the mass sheet degeneracy. Near the Einstein ring where we observe the hosts, the surface density of the SIE is $\kappa \simeq 0.5$ while that of a typical constant mass-to-light ratio \mathcal{M}/L model for the lens would be $\kappa \simeq 0.2$ because the SIE mass distribution is more centrally concentrated. The SIE model magnifies hosts more than the constant \mathcal{M}/L model, so if galaxies lacked dark matter we would underestimate their intrinsic fluxes by roughly $(1 - 0.2)^2 / (1 - 0.5)^2 \simeq 2.5$ or 1 magnitude. In practice, we know from studies of individual lenses (e.g. Impey et al. 1998; Lehar et al. 2000; Muñoz, Kochanek, & Keeton 2001), statistical properties of lens samples (e.g. Chae et al. 2002, Zhang 2004, Chen 2005, Rusin & Kochanek 2005), and dynamical studies (Rix et al. 1997, Treu & Koopmans 2004, Treu et al. 2006), that the typical lens has a radial density distribution that is reasonably well modeled by an SIE in the region where we observe the host galaxies. There is likely to be a scatter about this typical model, but it is probably at a level of 0.1–0.2 mag that does not represent a significant contribution to our uncertainties given the other sources of error. In our comparisons with the unlensed hosts of Kukula et al. (2001) and Ridgway et al. (2001) we find that the properties of the lensed and unlensed hosts are mutually consistent, adding empirical confirmation to this assertion.

UNCERTAINTIES DUE TO MODELING COMPLEXITY

The lens modeling and the image fitting process required to simultaneously model everything seen in each image are a non-trivial challenge. The complexity of the models has some effect on our inferences about the hosts, but little effect on our conclusions, by examining the lenses shown in Figures 2–6. Remember that shifts in the host luminosity larger than ~ 1 mag are required to significantly affect our discussion.

Figures 2–4 show deep (5 orbit) images of HE 1104–1805 ($z_s = 2.32$), PG 1115+080 ($z_s = 1.72$), RXJ 0911+0551 ($z_s = 2.8$), and B 1600+434 ($z_s = 1.59$), while Figure 6 is the shallower (2 orbit) image of BRI 0952–0115 ($z = 4.5$). In each case, the host is readily visible after subtracting the quasar and has a spatial structure virtually impossible to mimic with PSF errors or a mismodeled lens galaxy. Because of our restriction on the diameter of the Einstein ring ($> 0''.8$), the quasar images and the lens galaxy are well-separated. Thus, even though we must use a 7-parameter model for the lens galaxy light profile, these parameters have little covariance with those of the host. For the less well-constrained lenses, two-image lenses with less well-detected hosts, there can be degeneracies in the lens model trading off the elliptical structure of the lens and the external shear. But these are degeneracies that must hold the pattern of ray deflections fixed relative to the data, so they have negligible effects on the inferred structure of the host.

Empirically, the covariances between the parameters for the lens galaxy and the lens model negligibly broaden the uncertainties in the host properties.

One of our primary concerns is inferring the host parameters in shallow images where the outer regions of the host may be poorly detected. We can test for problems by comparing the host properties derived from deep 5-orbit images shown in Figs. 2–4, to those derived from earlier single orbit images. Both the depth of the observations and the PSF have changed. For HE 1104–1805 and PG 1115+080 the host luminosities found from the deep images are 0–0.15 mag brighter and there are 10–20% changes in the estimated effective radii. Such changes are quite comparable to the effects we find from using different model PSFs. Where the host is significantly fainter, as in RXJ 0911+0511, the upper limit on the luminosity estimate from the shallow image is 0.15 mag brighter than in the deep image. B 1600+434 is our most extreme example of the lens and host emission overlapping. We also require a two-component bulge+disk model for the lens and need to mask the dust lane in the disk of the lens galaxy. The difference in host luminosity between the deep and shallow images is at worst 0.25 mag, caused partly by uncertainties in the bulge-to-disk ratio of the lens galaxy (it ranges from 0.5 to 2), and partly by the lens model. For instance, if we artificially change the lens bulge size by 50% in the deep image, our estimate of the host luminosity changes by 0.3 mag. We also find that the uncertainties in the structures of the lensed hosts are markedly less than those for the unlensed hosts. Presumably this is a combination of better resolving the hosts because of the magnification and distorting it into a shape that has significantly less correlation with the structure of the PSF. In short, modeling lensed hosts may appear fraught with uncertainties, but in practice we can estimate their parameters at least as well as for unlensed hosts and in some cases markedly better.

PROBLEMATIC OBJECTS

Several objects are problematic (marked by embedded \times symbol or a dotted circle/square in Figures 8 and 9). Here we discuss the reasons for the outliers and why we have excluded some objects from our sample.

4C 45.51 – this unlensed QSO from Kukula et al. (2001) is an extremely powerful radio source ($\sim 3 \times 10^{28}$ to $\sim 10^{29}$ W Hz $^{-1}$ from 151 MHz to 37 GHz, e.g. Wiren et al. 1992; Hales, Baldwin & Warner 1993) which implies such a high Eddington ratio ($\epsilon_{Edd} \approx 0.7$) that the source is probably beamed towards us. If beamed emission contributes to the optical continuum, then the BH mass estimate is suspect (see also P06).

MG 2016+112 – this lensed quasar is peculiar on two grounds. First, it is a narrow line quasar (NLQ), and local studies of NLQ (narrow-line Seyfert 1) find that many are radiating near the Eddington limit and may be beamed (e.g. Greene & Ho 2004, Bian & Zhao 2004, Botte et al. 2005). Indeed, Botte et al. (2005) find larger BH masses using the $\mathcal{M}_{BH-\sigma_*}$ technique than through the virial estimate, casting significant doubt on the reliability of BH mass estimates in NLQs. Second, the extended optical emission observed in MG 2016+112 is also associated with lensed X-ray emission (Chartas et al. 2001) and images of the radio jets (Koopmans et al. 2002), suggesting that some of the optical emission is related to extended emission from a jet rather than from the host galaxy.

RXJ 0921+4528 – Based on our models of the host galaxies, we have concluded that this system (shown as a dotted circle in Figure 8) is a binary quasar rather than a gravitational lens. This was already a concern of Muñoz et al. (2001); in our analysis we see no signs of an Einstein ring structure to the host galaxies. Treated as a lens, the host galaxy lies far from the general trends with an inferred mass deficit of $\Gamma(z) \approx 30$, while treated as a binary it has a mass deficit of $\Gamma(z) \approx 4$ that is typical of the other host galaxies at its redshift.

B 1422+231 – this lensed QSO is excluded because we only have an upper limit on the luminosity of the host. Viewed as a marginal detection, the host luminosity is consistent with the general correlations, but we do not include it in the analysis.

SBS 0909+532 – the host galaxy images in this system merge into the emission from the lens galaxy and we lack a PSF model that works well for these observations. Thus we probably underestimate the host luminosity. We do not include it in the analysis.

FBQ 0951+2635 – as with B 1600+434, the lens is an edge on, late-type spiral galaxy that must be modeled using both a bulge and a disk. Unfortunately, the system is also more compact than B 1600+434, so the photometric models are less stable. Problems with the photometric model are real but seem to be too small to explain the offset. For example, using a bulgeless model for the lens galaxy only increases the host luminosity by 0.4 mag, which still leaves the system 2.6 mag off the general trend. Similarly, \mathcal{M}_{BH} may be underestimated because the Mg II line used to estimate it is heavily contaminated by Fe line emission, but the magnitude of any potential error is too small to explain the offset.

REFERENCES

- | | |
|---|---|
| <p>Aretxaga, I., Terlevich, R. J., & Boyle, B. J. 1998, MNRAS, 296, 643</p> <p>Bade, N., Siebert, J., Lopez, S., Voges, W., & Reimers, D. 1997, A&A, 317, L13</p> | <p>Barth, A. J., Greene, J. E., & Ho, L. C. 2005, ApJ, 619, L151</p> <p>Baskin, A., & Laor, A. 2005, MNRAS, 356, 1029</p> <p>Bauer, A. E., Drory, E., Hill, G. J., & Feulner, G. 2005, ApJ, 621, 89</p> |
|---|---|

- Bettoni, D., Falomo, R., Fasano, G., & Govoni, F. 2003, *A&A*, 399, 869
 Bian, W., & Zhao, Y. 2004, *MNRAS*, 352, 823
 Blandford, R. D., & McKee, C. F. 1982, *ApJ*, 255, 419
 Boroson, T. A. 2003, *ApJ*, 585, 647
 Borys, C., Smail, I., Chapman, S. C., Blain, A. W., Alexander, D. M., & Ivison, R. J., *ApJ*, 635, 853
 Botte, V., Ciroi, S., di Mille, F., Rafanelli, P., & Romano, A. 2005, *MNRAS*, 356, 789
 Bruzual, G., & Charlot, S. 2003, *MNRAS*, 344, 1000
 Cappellari, M., et al. 2005, *astro-ph/0505042*
 Chae, K.-H., et al. 2002, *Physical Review Letters*, 89, 151301
 Chartas, G. Bautz, M., Garmire, G., Jones, C., & Schneider, D. P., 2001, *ApJL*, 550, 163
 Chavushyan, V. H., Vlasyuk, V. V., Stepanian, J. A., & Erastova, L. K. 1997, *A&A*, 318, 67
 Chen, D.-M. 2005, *ApJ*, 629, 23
 Claeskens, J.-F., Surdej, J., & Remy, M. 1996, *A&A*, 305, L9
 Coleman, G. D., Wu, C.-C., & Weedman, D. W. 1980, *ApJS*, 43, 393
 Cox, P., et al. 2002, *A&A*, 387, 406
 Devriendt, J. E. G., Guiderdoni, B., & Sadat, R. 1999, *A&A*, 350, 381
 Di Matteo, T., Springel, V., & Hernquist, L. 2005, *Nature*, 433, 604
 Doyon, R., et al. 1994, *ApJ*, 437, 23
 Dunlop, J. S., McLure, R. J., Kukulka, M. J., Baum, S. A., O'Dea, C. P., & Hughes, D. H. 2003, *MNRAS*, 340, 1095
 Erwin, P., Graham, A. W., & Caon, N. 2002, *astro-ph/0212335*
 Falco, E. E., et al. 1999, *ApJ*, 523, 617
 Falomo, R., Kotilainen, J., & Treves, A. 2001, *ApJ*, 547, 124
 Fassnacht, C. D., & Cohen, J. 1998, *AJ*, 115, 377
 Fassnacht, C. D., et al. 1999, *AJ*, 117, 658
 Ferrarese, L., & Merritt, D. 2000, *ApJ*, 539, L9
 Ferrarese, L., Pogge, R. W., Peterson, B. M., Merritt, D., Wandel, A., & Joseph, C. L. 2001, *ApJ*, 555, 79
 Feulner, G., Goranova, Y., Drory, N., Hopp, U., & Bender, R. 2005, *MNRAS*, 358, 1
 Gebhardt, K., et al. 2000a, *ApJ*, 539, L13
 ——. 2000b, *ApJ*, 543, L5
 Gehren, T., Fried, J., Wehinger, P. A., & Wyckoff, S. 1984, *ApJ*, 278, 11
 Gómez-Alvarez, P. 2005, Conference on "25 Years After Discovery: Some Current Topics on Lensed QSOs", Ed. L. J. Goicoechea (UC, Spain), p. 23
 Graham, A. W., Erwin, P., Caon, N., & Trujillo, I. 2001, *ApJ*, 563, 11
 Greene, J. E., & Ho, L. C. 2004, *ApJ*, 610, 722
 Greene, J. E., & Ho, L. C. 2005, *astro-ph/0512461*
 Hammer, F., Rigaut, F., Angonin-Willaime, M.-C., & Vanderriest, C. 1995, *A&A*, 298, 737
 Häring, N., & Rix, H.-W. 2004, *ApJ*, 604, 89
 Hales, S. E. G., Baldwin, J. E., & Warner, P. J., 2003, *MNRAS*, 263, 25
 Hewett, P. C., Irwin, M. J., Foltz, C. B., Harding, M. E., Corrigan, R. T., Webster, R. L., & Dinshaw, N., 1994, *AJ*, 108, 1534
 Ho, L. C. 1999, in *Observational Evidence for Black Holes in the Universe*, ed. S. K. Chakrabarti (Dordrecht: Kluwer), 157
 Ho, L. C. 2002, *ApJ*, 564, 120
 Ho, L. C. 2005, *ApJ*, 629, 680
 Hogg, D. W., Baldry, I. K., Blanton, M. R., & Eisenstein, D. J. 2004, *astro-ph/0210394*
 Hutchings, J. B., Crampton, D., & Campbell, B. 1984, *ApJ*, 280, 41
 Hutchings, J. B., Frenette, D., Hanisch, R., Mo, J., Dumont, P. J., Redding, D. C., & Neff, S. G. 2002, *AJ*, 123, 2936
 Hutchings, J. B. 2003, *AJ*, 125, 1053
 Impey, C. D., Falco, E. E., Kochanek, C. S., Lehár, J., McLeod, B. A., Rix, H.-W., Peng, C. Y., & Keeton, C. R. 1998, *ApJ*, 509, 551
 Inada, N. et al. 2003, *AJ*, 126, 666
 Isaak, K. G., Priddey, R. S., McMahon, R. G., Beelen, A., Peroux, C., Sharp, R. G., & Withington, S. 2002, *MNRAS*, 329, 149
 Ivanov, V. D., & Alonso-Herrero, A. 2003, *Ap&SS*, 284, 565
 Jahnke, K. et al. 2004, *ApJ*, 614, 568
 Kaspi, S., Smith, P. S., Netzer, H., Maoz, D., Jannuzi, B. T., & Givon, U. 2000, *ApJ*, 533, 631
 Kaspi, S., Maoz, D., Netzer, H., Peterson, B. M., Vestergaard, & M., Jannuzi, B. T. 2005, *ApJ*, 629, 61
 Keeton, C. R., Kochanek, C. S., & Seljak, U. 1997, *ApJ*, 482, 604
 Keeton, C. R. et al. 2000, *ApJ*, 542, 74
 Keeton, C. R., Burles, S., Schechter, P., & Wambsganss, J. 2005, *ApJin press*
 Kochanek, C. S., Falco, E. E., Impey, C. D., Lehár, J., McLeod, B. A., & Rix, H.-W. 1999, in *After the Dark Ages: When Galaxies were Young (the Universe at $2 \leq z \leq 5$)*, ed. S. Holt & E. Smith (New York: AIP), 163
 Kochanek, C. S., Keeton, C. R., & McLeod, B. A. 2001, *ApJ*, 547, 50
 Kochanek, C. S., Schneider, P., Wambsganss, J., 2004, Part 2 of *Gravitational Lensing: Strong, Weak & Micro*, Proceedings of the 33rd Saas-Fee Advanced Course, G. Meylan, P. Jetzer & P. North, eds. (Springer-Verlag: Berlin)
 Kollmeier, J. et al. 2005, *ApJ submitted*
 Koopmans, L. V. E., Garrett, M. A., Blandford, R. D., Lawrence, C. R., Patnaik, A. R., & Porcas, R. W., 2002, *MNRAS*, 334, 39
 Koopmans, L. V. E., Treu, T., Fassnacht, C. D., Blandford, R. D., & Surpi, G. 2003, *ApJ*, 599, 70
 Koopmans, L. V. E., & Treu, T. 2004, *Multiwavelength Cosmology*. Proceedings of the "Multiwavelength Cosmology" conference, held on Mykonos Island, Greece, 17-20 June, 2003. Ed. Manolis Plionis. *ASTROPHYSICS AND SPACE SCIENCE LIBRARY* Vol. 301., Pub. Kluwer Academic Publishers, Dordrecht, The Netherlands, 2004, p.23, 23
 Kormendy, J. 2004, in *Carnegie Observatories Astrophysics Series, Vol. 1: Coevolution of Black Holes and Galaxies*, ed. L. C. Ho (Cambridge: Cambridge Univ. Press), in press.
 Kormendy, J., & Gebhardt, K. 2001, in *20th Texas Symposium on Relativistic Astrophysics*, ed. H. Martel & J. C. Wheeler (Melville: AIP), 363
 Kormendy, J., & Richstone, D. 1995, *ARA&A*, 33, 581
 Kuhlbrodt, B., Orndahl, E., Wisotzki, L., & Jahnke, K. 2005, *astro-ph/0503284*
 Kukulka, M., Dunlop, J. S., McLure, R. J., Miller, L., Percival, W. J., Baum, S. A., & O'Dea, C. P. 2001, *MNRAS*, 326, 1533
 Kundić, T., Cohen, J. G., Blandford, R. D., & Lubin, L. M. 1997, *AJ*, 114, 507
 Labbé, I., et al. 2005, *ApJ*, 624, 81
 Lacy, M., Gates, E. L., Ridgway, S. E., de Vries, W., Canalizo, G., Lloyd, J. P., & Graham, J. R. 2002, *AJ*, 124, 3023
 Laor, A. 2001, *ApJ*, 553, 677
 Lawrence, C. R., Elston, R., Januzzi, B. T., & Turner, E. L. 1995, *AJ*, 110, 2570
 Lawrence, A. 1999, *Advances in Space Research*, v. 23, 5-6, 1167
 Lehár, J., Falco, E. E., Kochanek, C. S., McLeod, B. A., Muñoz, J. A., Impey, C. D., Rix, H.-W., Keeton, C. R., & Peng, C. Y. 2000, *ApJ*, 536, 854
 Lehnert, M. D., Heckman, T. M., Chambers, K. C., & Miley, G. K. 1992, *ApJ*, 393, 68
 Lehnert, M. D., van Breugel, W. J. M., Heckman, T. M., & Miley, G. K. 1999, *ApJS*, 124, 11
 Lonsdale, C., Farrah, D., & Smith, H. 2006, Review Article, "Astrophysics Update 2 - topical and timely reviews on astronomy and astrophysics." Ed. J. W. Mason, Springer/Praxis books. ISBN: 3-540-30312-X
 MacAlpine, G. M., & Feldman, F. R. 1982, *ApJ*, 261, 412
 Magorrian, J., et al. 1998, *AJ*, 115, 2285
 Marconi, A., & Hunt, L. K. 2003, *ApJ*, 589, L21
 McLeod, K. K., & Rieke G. H. 1994, *ApJ*, 420, 58
 McLeod, K. K. 1995, *PASP*, 107, 91
 McLeod, K. K., & Rieke G. H. 1995, *ApJ*, 454, L77
 McLeod, K. K., & McLeod, B. A. 2001, *ApJ*, 546, 782
 McLure, R. J., Kukulka, M. J., Dunlop, J. S., Baum, S. A., O'Dea, C. P., & Hughes, D. H. 1999, *MNRAS*, 308, 377
 McLure, R. J., & Dunlop, J. S. 2002, *MNRAS*, 331, 795
 McLure, R. J., & Jarvis, M. J. 2002, *MNRAS*, 337, 109
 McLure, R. J., et al. 2005, *astro-ph/0510121*
 Merloni, A., Rudnick, G., & Di Matteo, T. 2004, *MNRAS*, 354, 37
 Merritt, D., & Ferrarese, L. 2001, *MNRAS*, 320, L30
 Monier, E. M., Turnshek, D. A., & Lupie, O. L. 1998, *ApJ*, 496, 177
 Morgan, N. D., Becker, R. H., Gregg, M. D., Schechter, P. L., & White, R. L. 2001, *AJ*, 121, 611
 Muñoz, J. A., Falco, E. E., Kochanek, C. S., Lehár, J., Herold, L. K., Fletcher, A. B., & Burke, B. F. 1998, *ApJ*, 492, 9
 Muñoz, J. A., et al. 2001, *ApJ*, 546, 769
 Muñoz, J. A., Kochanek, C. S., Keeton, C. R. 2001, *ApJ*, 558, 657
 Muñoz, J. A., Falco, E. E., Kochanek, C. S., McLeod, B. A., Mediavilla, E. 2004, *ApJ*, 605, 614
 Nelson, C. H., 2000, *ApJ*, 544, 91

- Nelson, C. H., Green, R. F., Bower, G., Gebhardt, K., & Weistrop, D. 2004, *ApJ*, 615, 652
- Netzer, H. 2003, *ApJ*, 583, L5
- Neugebauer, G., Matthews, K., Soifer, B. T., & Elias, J. H. 1985, *ApJ*, 298, 275
- Oguri, M., et al. 2004, *PASJ*, 56, 399
- Onken, C. A. et al. 2004, *ApJ*, 615, 645
- Oscz, A., Serra-Ricart, M., Medivilla, E., Buitrago, J., & Goicoechea, L. J. 1997, *ApJ*, 491, L7
- Ouchi, M. et al. 2004, *ApJ*, 611, 660
- Peng, C. Y., Ho, L. C., Impey, C. D., & Rix, H.-W. 2002, *AJ*, 124, 266
- Peng, C. Y., Impey, C. D., Ho, L. C., Barton, E. J., & Rix, H.-W. 2006, *ApJ*, 640, 114 [P06]
- Peterson, B. M. 1993, *PASP*, 105, 247
- Peterson, B. M. et al. 2004, *ApJ*, 613, 682
- Popović, L. C., et al. 2006, *ApJ*, 637, 620
- Press, W. H., Teukolsky, S. A., Vetterling, W. T., & Flannery, B. P. 1992, *Numerical Recipes in Fortran* (2nd Ed.; Cambridge: Cambridge Univ. Press)
- Reddy, N. A., Steidel, C., & Erb, D. 2005, in "Starbursts: From 30 Doradus to Lyman Break Galaxies", eds. R. de Grijs & R. M. González Delgado, *Astrophysics & Space Science Library*, Vol. 329, Dordrecht: Springer, 205, p. 65
- Reddy, N. A., et al. 2006, *astro-ph/0602596*
- Richards, G. T., et al. 2004, *ApJ*, 610, 679
- Ridgway, S. E., Heckman, T. M., Calzetti D., & Lehnert, M. 2001, *ApJ*, 550, 122
- Rix, H.-W., de Zeeuw, P. T., Cretton, N., van der Marel, R. P., & Carollo, C. M. 1997, *ApJ*, 488, 702
- Rudnick, G., et al. 2003, *ApJ*, 599, 847
- Rusin, D. & Kochanek, C. S. 2005, *ApJ*, 623, 666
- Sánchez, S. F., & González-Serrano, J. I. 2003, *A&A*, 406, 435
- Sánchez, S. F., et al. 2004, *ApJ*, 614, 586
- Schechter, P., L., Gregg, M. D., Becker, R. H., Helfand, D. J., & White, R. L. 1998, *ApJ*, 115, 1371
- Schlegel, D. J., Finkbeiner, D. P., & Davis, M. 1998, *ApJ*, 500, 525
- Schneider, D. P., Lawrence, C. R., Schmidt, M., Gunn, J. E., Turner, E. L., Burke, B. F., & Dhawan, V. 1985, *ApJ*, 294, 66
- Schneider, P., Ehlers, J., & Falco, E. E. 1992, *Gravitational Lenses*, XIV, 560 pp. 112 figs.. Springer-Verlag Berlin Heidelberg New York. Also *Astronomy and Astrophysics Library*.
- Shapley, A. E., et al. 2001, *ApJ*, 562, 95
- Shapley, A. E., Steidel, C. C., Erb, D. K., Reddy, N. A., Adelberger, K. L., Pettini, M., Barmby, P., & Huang, J. 2005, *ApJ*, 626, 698
- Shields, G. A. et al. 2003, *ApJ*, 583, 124
- Shields, G. A., Salviander, S., Bonning, E. W. 2006, *astro-ph/0601675*
- Sluse, D., et al. 2003, *A&A*, 406, 43
- Storrie-Lombardi, L. J., McMahon, R. G., Irwin, M. J., & Hazard, C. 1996, *ApJ*, 468, 121
- Surpi, G., & Blandford, R. D. 2003, *ApJ*, 584, 100
- Treu, T., & Koopmans, L. V. E. 2004, *ApJ*, 611, 739
- Treu, T., Malkan, M. A., & Blandford, R. D. 2004, *ApJ*, 615, 97
- Treu, T., et al. 2005, *astro-ph/0512044*
- van Dokkum, P. G., & Franx, M. 2001, *ApJ*, 553, 90
- Véron-Cetty, M.-P., Véron, P. 1996, *ESO Sci. Rep. No. 17*. ESO Publications, Garching
- Vestergaard, M. 2002, *ApJ*, 571, 733
- Vestergaard, M. 2004, *ApJ*, 601, 676
- Vestergaard, M., & Peterson, B. M. 2006, *ApJ*, 641, 689
- Wandel, A., Peterson, B. M., & Malkan, M. A. 1999, *ApJ*, 526, 579
- Wang, Y. P., Biermann, P. L., & Wandel, A. 2000, *A&A*, 361, 550
- Wayth, R. B., O'Dowd, M., & Webster, R. L. 2005, *MNRAS*, 359, 561
- Winn, J. N., et al. 2002, *AJ*, 123, 10
- Wiren, S. et al. 1992, *AJ*, 104, 1009
- Wisotzki, L., Köhler, T., Ikonou, M., & Reimers, D. 1995, *A&A*, 297, L59
- Wisotzki, L., Köhler, T., Lopez, S., & Reimers, D. 1996, *A&A*, 315, L405
- Wisotzki, L., Schechter, P. L., Bradt, H. V., Heinmüller, & Reimers, D. 2002, *A&A*, 395, 17
- Wisotzki, L., Schechter, P. L., Chen, H. W., Richstone, D., Jahnke, K., Sánchez, S. F., & Reimers, D. 2004, *A&A*, 419, 31
- Woo, J.-H., & Urry, C. M. 2002, *ApJ*, 579, 530
- Yoo, J., Kochanek, C. S., Falco, E. E., & McLeod, B. A. 2005, *astro-ph/0511001*
- Young, P., Sargent, W. L. W., Boksenberg, A., & Oke, J. B. 1981, *ApJ*, 249, 415
- Zhang, T.-J. 2004, *ApJ*, 602, L5
- Zitelli, V., Mignoli, M., Zamorani, G., Marano, B., & Boyle, B. J. 1992, *MNRAS*, 256, 349

TABLE 1
QUASAR AND HOST GALAXY DATA FROM CASTLES

Object	z_s	Size (")	RA (J2000)	DEC (J2000)	A_H (mag)	Host (mag)	Quasar (mag)	RLQ?	Comments
(1)	(2)	(3)	(4)	(5)	(6)	(7)	(8)	(9)	(10)
CTQ 414	1.29	1.22	01:58:41.44	-43:25:04.20	0.01	19.87	18.09	?	See Peng et al. (2005)
B 0712+472	1.34	1.46	07:16:03.58	+47:08:50.0	0.07	19.89	23.67	Y	Lens edge on disk?
SBS 0909+532	1.38	1.17	09:13:01.05	+52:59:28.83	0.01	20.89	16.41	?	
FBQ 0951+2635	1.24	1.11	09:51:22.57	+26:35:14.1	0.01	21.07	16.57	?	Lens edge on disk
Q 0957+561	1.41	6.26	10:01:20.78	+55:53:49.4	0.01	17.83	17.05	Y	
LBQS 1009-0252c	1.63	—	10:12:15.83	-03:07:01.6	0.02	19.41	17.90	?	Not lensed
B 1030+071	1.54	1.56	10:33:34.08	+07:11:25.5	0.01	19.93	19.15	Y	
RXJ 1131-1231	0.66	3.69	11:31:51.6	-12:31:57	0.02	17.48	19.25	?	B/D decomposition done
SDSS 1226-0006	1.12	1.20	12:26:08.10	-00:06:02.0	0.01	19.77	18.93	?	
SDSS 1335+0118	1.57	1.57	13:35:34.79	+01:18:05.5	0.01	20.24	17.49	?	
B 1600+434	1.59	1.40	16:01:40.45	+43:16:47.8	0.01	20.23	21.43	Y	Lens edge on disk
FBQ 1633+3134	1.52	0.75	16:33:48.99	+31:34:11.90	0.02	19.84	16.84	?	
B 2045+265	1.28	2.76	20:47:20.35	+26:44:01.2	0.13	22.81	24.98	Y	
MGC 2214+3550 A	0.88	—	22:14:57.04	+35:51:25.5	0.07	18.03	19.16	Y	Not lensed
MGC 2214+3550 B	0.88	—	22:14:57.04	+35:51:25.5	0.07	19.16	20.08	Y	Not lensed
HE 0047-1756	1.66	1.44	00:50:27.83	-17:40:8.8	0.01	19.72	18.25	?	
Q 0142-110	2.72	2.24	00:49:41.89	-27:52:25.7	0.02	21.01	16.55	?	
MG 0414+0534	2.64	2.40	04:14:37.73	+05:34:44.3	0.18	20.78	18.63	Y	
HE 0435-1223	1.69	2.43	04:38:14.9	-12:17:14.4	0.03	20.09	19.64	?	
RXJ 0911+0551	2.80	2.47	09:11:27.50	+05:50:52.0	0.03	22.23	20.23	?	
RXJ 0921+4528	1.65	—	09:21:12.81	+45:29:04.4	0.01	20.01	16.95	?	Not lensed?
RXJ 0921+4528	1.65	—	09:21:12.81	+45:29:04.4	0.01	19.34	18.36	?	Not lensed?
SDSS 0924+0219	1.54	1.74	09:24:55.87	+02:19:24.9	0.03	19.85	21.00	?	
BRI 0952-0115	4.5	1.00	09:55:00.01	-01:30:05.0	0.01	22.29	19.10	?	
J 1004+1229	2.65	1.54	10:04:24.9	+12:29:22.3	0.02	20.08	17.28	?	
LBQS 1009-0252	2.74	1.54	10:12:15.71	-03:07:02.0	0.02	20.75	17.75	?	
Q 1017-207	2.55	0.85	10:17:24.13	-20:47:00.4	0.03	19.94	17.29	?	
HE 1104-1805	2.32	3.19	11:06:33.45	-18:21:24.2	0.03	20.14	18.27	?	
PG 1115+080	1.72	2.32	11:18:17.00	+07:45:57.7	0.02	20.23	18.80	?	
H 1413+117	2.55	1.35	14:15:46.40	+11:29:41.4	0.01	20.47	18.41	?	
B 1422+231	3.62	1.68	14:24:38.09	+22:56:00.6	0.03	[21]	16.71	Y	Upper limit on host
SBS 1520+530	1.86	1.59	15:21:44.83	+52:54:48.6	0.01	21.09	19.01	?	Lens edge on disk
PMNJ 1632-0033	3.42	1.47	16:32:57.68	-00:33:21.1	0.06	22.25	19.59	?	
MG 2016+112	3.27	3.52	20:19:18.15	+11:27:08.3	0.14	22.35	21.47	Y	NL QSO
HE 2149-2745	2.03	1.70	21:52:07.44	-27:31:50.2	0.02	19.75	16.85	?	
PSS 2322+1944	4.1	1.50	23:22:07.2	+19:44:23	0.03	21.83	18.99	?	

NOTE. — Col. (1): Object name. Col. (2): Quasar redshift. Col. (3): Estimated angular diameter of lensing geometry. Col. (4): RA (J2000). Col. (5): DEC (J2000). Col. (6): Extinction in H -band. Col. (7): Intrinsic (i.e. lens deprojected) H -band host magnitude. The typical uncertainties are 0.3 mag. Col. (8): Intrinsic H -band quasar magnitude. Col. (9): Radio loud quasar? Objects with “?” do not have known radio observations. Col. (10): Comments.

TABLE 2
 QUASAR AND HOST GALAXY DATA COMPILED FROM THE LITERATURE

Object (1)	z (2)	Filter (3)	NICMOS Mag				Quasar		Radio Loud? (10)	References/Comments (11)
			Host (4)	Err (5)	Quasar (6)	Err (7)	Filter (8)	Mag (9)		
SGP5:46	0.955	F110M	20.09	0.4	19.45	0.3	V^*	19.7	N	1, assumed quasar ($B - V$)=0.3
PKS 0440-00	0.844	F110M	18.79	0.4	18.42	0.3	V^*	19.1	Y	1
PKS 0938+18	0.943	F110M	19.46	0.4	19.78	0.3	V	18.9	Y	1, assumed quasar ($B - V$)=0.3
3C 422	0.942	F110M	18.24	0.4	17.85	0.3	V	18.9	Y	1, assumed quasar ($B - V$)=0.3
SGP2:11	1.976	F165M	20.64	0.75	18.96	0.3	B^*	20.9	N	1
SGP2:25	1.868	F165M	19.88	0.75	19.59	0.3	B^*	20.7	N	1
SGP2:36	1.756	F165M	19.73	0.75	19.97	0.3	B^*	20.7	N	1
SGP3:39	1.964	F165M	19.75	0.75	19.53	0.3	B^*	20.8	N	1
SGP4:39	1.716	F165M	21.59	0.75	18.85	0.3	B^*	20.8	N	1
4C 45.51	1.992	F165M	17.79	0.75	17.41	0.3	B	20.1	Y	1
MZZ 9744	2.735	F160W	21.73	0.5	20.02	0.05	B^*	21.4	N	2
MZZ 9592	2.710	F160W	20.70	0.1	19.57	0.03	B^*	21.8	N	2
MZZ 1558	1.829	F165M	20.64	0.2	19.08	0.04	B^*	21.5	N	2
MZZ 11408	1.735	F165M	20.78	0.4	21.08	0.06	B^*	21.9	N	2
MZZ 4935	1.876	F165M	22.00	0.4	21.23	0.06	B^*	21.8	N	2

NOTE. — Col. (1): Object name. Col. (2): Redshift. Col. (3): *HST* Filter. Col. (4-7): Apparent magnitude and their published uncertainties, in the Vega magnitude system, corrected for extinction from Schlegel et al. (1998). The values are taken from Kukula et al. (2001), Ridgway et al. (2001), and corrected slightly by P06 for morphology assumptions. Col. (8/9): Quasar magnitude (corrected for extinction), in the Vega magnitude system, corresponding to the filter in Col. (8). Filters with superscript * are photographic magnitudes. The B and V -band magnitudes of the quasars in Kukula et al. (2001) sample are from Véron-Cetty & Véron (1996), and references therein, while the B -band magnitudes for MZZ objects are from Zitelli et al. (1992). Where V -band magnitude is needed and unavailable, we used $(B - V) = 0.3$, which corresponds to $f_\nu \propto \nu^{-0.5}$. Col. (10): Radio-loud quasar or radio-quiet quasar. Col. (11): The photometry for each set of objects comes from the references shown. References.— (1) Kukula et al. 2001; (2) Ridgway et al. 2001.

TABLE 3
 QUASAR AND HOST GALAXY DERIVED QUANTITIES FROM CASTLES DATA

Object	z_s	Diameter	Host	Quasar Related Quantities					\mathcal{M}_{BH}	Comments/References
(1)	(2)	['']	M_R [mag]	M_B [mag]	Line(s) used	FWHM [Å]	$\log(\lambda L_\lambda(\text{cont}))$ $\log([\text{ergs s}^{-1}])$	Spectral slope n	[$10^9 \mathcal{M}_\odot$]	(11)
CTQ 414	1.29	1.22	-22.77	-24.19	C IV/Mg II	40/40	45.53/45.31	-1.65	0.34/0.16	See Peng et al. (2005)
B 0712+472	1.34	1.46	-22.86	-17.90	Mg II	110	42.74	0	0.07	1, Lens edge on disk?
SBS 0909+532	1.38	1.17	-21.95	-25.70	Mg II	138	45.95	-0.95	3.87	2, Confusion lim./PSF issues
SDSS 0924+0219	1.54	1.74	-23.32	-21.78	Mg II	61	44.35	-1.9	0.11	3
FBQ 0951+2635	1.24	1.11	-21.22	-25.66	Mg II	70	45.90	-1.73	0.89	4, Lens edge on disk
Q 0957+561	1.41	6.26	-25.08	-27.00	C IV/Mg II	50/100	46.71/46.43	-1.8	2.01/3.02	5
LBQS 1009-0252c	1.63	—	-23.94	-25.07	C IV	71	46.11	-2.1	1.64	6, Not lensed
B 1030+071	1.54	1.56	-23.25	-23.27	Mg II	86	44.82	-1.0	0.35	1
RXJ 1131-1231	0.66	3.69	-23.14	-20.90	H β	90	43.95	-1.0	0.06	7
SDSS 1226-0006	1.12	1.20	-22.44	-22.70	Mg II	120	44.48	-0.6	0.68	
SDSS 1335+0118	1.57	1.57	-23.03	-25.17	Mg II	120	45.60	-1.0	1.55	8
B 1600+434	1.59	1.40	-23.04	-21.41	Mg II	63	44.23	-1.9	0.10	1, Lens edge on disk
FBQ 1633+3134	1.52	0.75	-23.30	-25.85	C IV/Mg II	65/104	46.24/45.98	-1.75	1.76/1.84	9
B 2045+265	1.28	2.76	-19.80	-15.91	Mg II	78	41.49	1.3	0.01	10
MGC 2214+3550 A	0.88	—	-23.42	-21.82	Mg II	160	44.46	[-1.5]	1.64	11, Not lensed
MGC 2214+3550 B	0.88	—	-22.08	-20.97	Mg II	110	44.08	[-1.5]	0.43	11, Not lensed
HE 0047-1756	1.66	1.44	-23.69	-24.75	C IV	70	46.07	-2.1	1.48	12
Q 0142-110	2.72	2.24	-24.02	-27.37	C IV	75	46.85	-1.75	2.26	13, line center absorbed
MG 0414+0534	2.64	2.40	-24.13	-25.22	H β	262	45.73	1	1.82	14
HE 0435-1223	1.69	2.43	-23.40	-23.29	C IV	70	45.19	-1.7	0.50	15
RXJ 0911+0551	2.80	2.47	-22.93	-23.73	C IV	100	45.57	-2.07	0.80	16
RXJ 0921+4528A	1.65	6.97	-23.39	-25.95	C IV/Mg II	52/141	46.31/46.03	-1.8	1.10/3.21	17, Excl. from fit: not lensed?
RXJ 0921+4528B	1.65	6.97	-24.06	-24.54	C IV/Mg II	52/141	45.74/45.46	-1.8	0.55/1.74	17, Excl. from fit: not lensed?
BRI 0952-0115	4.5	1.00	-25.47	-26.09	C IV	146	46.00	-1.1	1.39	18
J 1004+1229	2.65	2.65	-24.86	-26.58	C IV	91	46.41	-1.5	2.02	19
LBQS 1009-0252	2.74	1.54	-24.31	-26.19	C IV/Mg II	75/100	46.27/46.08	-1.55	1.11/0.86	6
Q 1017-207	2.55	0.85	-24.83	-26.49	C IV	80	46.42	-1.6	1.68	20
HE 1104-1805	2.32	3.19	-24.31	-25.35	C IV	103	46.18	-2.02	2.37	21
PG 1115+080	1.72	2.32	-23.29	-24.24	C IV/Mg II	69/127	45.74/45.39	-2.02	0.92/1.23	22
H 1413+117	2.55	1.35	-24.30	-25.35	C IV	52	45.61	-0.9	0.26	23, BALQSO
B 1422+231	3.62	1.68	[-24.6]	-27.90	C IV/Mg II	133/139	46.88/46.74	-1.4	4.79/2.23	24, Excl. from fit: non-det.
SBS 1520+530	1.86	1.59	-22.66	-24.16	C IV	75	45.64	-1.9	0.88	25, Lens edge on disk
PMNJ 1632-0033	3.42	1.47	-23.97	-24.84	C IV	100	45.22	-0.7	0.39	26
MG 2016+112	3.27	3.52	-23.59	-23.00	C IV	25	44.56	-0.7	0.01	27, Excl. from fit: NLQSO
HE 2149-2745	2.03	1.70	-24.27	-26.52	C IV	117	46.67	-2.05	6.62	28, BALQSO
PSS 2322+1944	4.1	1.50	-25.48	-25.8	$\epsilon_{\text{Edd}}=1$	N/A	N/A	N/A	$\gtrsim 2.36$	29

NOTE. — Values in square brackets [] indicate that they are held fixed. Col. (1): Object name. Col. (2): Quasar redshift. Col. (3): Estimated angular diameter of lensing geometry. Col. (4): Inferred host restframe absolute R -band magnitude based on Sbc SED. Col. (5): Inferred quasar restframe B -band magnitude. Col. (6): Emission line(s) used to infer \mathcal{M}_{BH} . Col. (7): Observed-frame FWHM of emission line in Col. 6. Col. (8): Monochromatic continuum luminosity appropriate for corresponding lines used in Col. 6: for C IV, $\lambda L_\lambda(1350 \text{ \AA})$; for Mg II, $\lambda L_\lambda(3000 \text{ \AA})$; for H β , $\lambda L_\lambda(5100 \text{ \AA})$. Col. (9): Continuum spectral slope n in λ^n used to extrapolate values in Cols. 5 and 8. Col. (10): Black hole masses using the virial technique, using the corresponding lines in Col. 6. For PSS 2322+1944, \mathcal{M}_{BH} is based on Eddington limited accretion in Isaak et al. (2002), corrected for lensing magnification. Thus it is a lower limit. Col. (11): Comments and References from which spectral information was obtained — 1. Fassnacht & Cohen (1998), 2. Oscoz et al. (1997), 3. Inada et al. (2003), 4. Schechter et al. (1998), 5. Young et al. (1981), 6. Hewett et al. (1994), 7. Sluse et al. (2003), 8. Oguri et al. (2004), 9. Morgan et al. (2001), 10. Fassnacht et al. (1999), 11. Muñoz et al. (1998), 12. Wisotzki et al. (2004), 14. MacAlpine & Feldman (1982), 14. Lawrence et al. (1995), 15. Wisotzki et al. (2002), 16. Bade et al. (1997), 17. Muñoz et al. (2001), 18. Storrie-Lombardi et al. (1996), 19. Gómez-Alvarez (2005), 20. Claeskens, Surdej, & Remy (1996), 21. Wisotzki et al. (1995), 22. Kundić et al. (1997), 23. Monier, Turnshek, & Lupie (1998), 24. Hammer et al. (1995), 25. Chavushyan et al. (1997), 26. Winn, J. N., et al. (2002), 27. Schneider et al. (1985), 28. Wisotzki et al. (1996), 29. Cox, P., et al. (2002),

TABLE 4
 QUASAR AND HOST GALAXY DERIVED QUANTITIES FROM THE LITERATURE

Object (1)	z_s (2)	Host M_R [mag] (3)	M_B [mag] (4)	Quasar Related Quantities				\mathcal{M}_{BH} [$10^9 \mathcal{M}_{\odot}$] (9)	Comments (10)
				Line(s) used (5)	FWHM [\AA] (6)	$\log(\lambda L_{\lambda}(\text{cont}))$ $\log([\text{ergs s}^{-1}])$ (7)	Spectral slope n (8)		
SGP5:46	0.955	-22.90	-23.04	Mg II	55	44.96	-2.2	0.16	Narrow line Mg II
PKS 0440-00	0.844	-23.83	-23.69	Mg II	50	45.16	-1.9	0.18	Narrow line Mg II
PKS 0938+18	0.943	-23.49	-22.76	Mg II	100	44.90	-2.5	0.49	
3C 422	0.942	-24.71	-24.39	Mg II	140	45.36	-1.4	1.58	Heavily absorbed Mg II
SGP2:11	1.976	-23.19	-24.20	C IV	90	45.57	-1.7	1.06	
SGP2:25	1.868	-23.77	-23.56	C IV	70	45.48	-2.0	0.61	
SGP2:36	1.756	-23.75	-23.22	C IV	100	45.61	-2.5	1.58	
SGP3:39	1.964	-24.05	-23.76	C IV	85	45.66	-2.2	1.06	
SGP4:39	1.716	-21.82	-24.00	C IV	45	45.38	-1.5	0.25	
4C 45.51	1.992	-26.06	-25.66	C IV/Mg II	58/101	45.90/45.83	-1.2	0.65/0.58	
MZZ 9744	2.735	-23.33	-23.91	C IV	90	45.62	-2.0	0.71	
MZZ 9592	2.71	-24.32	-24.35	C IV	90	45.52	-1.5	0.63	C IV partly absorbed
MZZ 1558	1.829	-22.95	-23.82	C IV	120	45.22	-1.3	1.34	
MZZ 11408	1.735	-22.66	-22.07	C IV	50	45.09	-2.4	0.21	
MZZ 4935	1.876	-21.67	-22.11	C IV	50	45.21	-2.6	0.22	

NOTE. — Col. (1): Object name. Col. (2): Quasar redshift. Col. (3): Inferred host restframe absolute R -band magnitude based on Sbc SED. Col. (4): Inferred quasar restframe B -band magnitude. Col. (5): Emission line(s) used to infer \mathcal{M}_{BH} . Col. (6): Observed-frame FWHM of emission line in Col. 5. Col. (7): Monochromatic continuum luminosity appropriate for corresponding lines used in Col. 6: for C IV, $\lambda L_{\lambda}(1350 \text{ \AA})$; for Mg II, $\lambda L_{\lambda}(3000 \text{ \AA})$. Col. (8): Continuum spectral slope n , in λ^n , used to extrapolate values in Cols. 4 and 7. Col. (9): Black hole masses using the virial technique, using the corresponding lines in Col. 5.